© 2021. Published by The Company of Biologists Ltd | Journal of Cell Science (2021) 134, jcs258523. doi:10.1242/jcs.258523

RESEARCH ARTICLE

The interaction of ATP11C-b with ezrin contributes to its polarized localization

Hiroki Inoue*,[1], Hiroyuki Takatsu*,[1], Asuka Hamamoto[1], Masahiro Takayama[1], Riki Nakabuchi[2], Yumeka Muranaka[2], Tsukasa Yagi[2], Kazuhisa Nakayama[1] and Hye-Won Shin[1,‡]

ABSTRACT

ATP11C, a member of the P4-ATPase family, translocates phosphatidylserine and phosphatidylethanolamine at the plasma membrane. We previously revealed that its C-terminal splice variant ATP11C-b exhibits polarized localization in motile cell lines, such as MDA-MB-231 and Ba/F3. In the present study, we found that the C-terminal cytoplasmic region of ATP11C-b interacts specifically with ezrin. Notably, the LLxY motif in the ATP11C-b C-terminal region is crucial for its interaction with ezrin as well as its polarized localization on the plasma membrane. A constitutively active, C-terminal phosphomimetic mutant of ezrin was colocalized with ATP11C-b in polarized motile cells. ATP11C-b was partially mislocalized in cells depleted of ezrin alone, and exhibited greater mislocalization in cells simultaneously depleted of the family members ezrin, radixin and moesin (ERM), suggesting that ERM proteins, particularly ezrin, contribute to the polarized localization of ATP11C-b. Furthermore, *Atp11c* knockout resulted in C-terminally phosphorylated ERM protein mislocalization, which was restored by exogenous expression of ATP11C-b but not ATP11C-a. These observations together indicate that the polarized localizations of ATP11C-b and the active form of ezrin to the plasma membrane are interdependently stabilized.

KEY WORDS: Actin, Biological membrane, Ezrin, Flippase, Polarization

INTRODUCTION

Cellular membranes exhibit transbilayer lipid asymmetry, which is regulated and maintained by lipid scramblases, floppases and flippases (Andersen et al., 2016; Bevers and Williamson, 2016; Coleman et al., 2013; Murate et al., 2015; Shin and Takatsu, 2019). Members of the P4-ATPase family translocate membrane lipids from the exoplasmic or luminal leaflet to the cytosolic leaflet (Andersen et al., 2016; Palmgren et al., 2019; Palmgren and Nissen, 2011; Shin and Takatsu, 2019). Among the P4-ATPases, ATP8B1, ATP8B2, ATP8B4, ATP10A, ATP10D, ATP11A and ATP11C primarily localize to the plasma membrane and possess flippase activities toward specific substrates, including phosphatidylserine (PS) and phosphatidylethanolamine (PE) for ATP11A and ATP11C; phosphatidylcholine for ATP8B1, ATP8B2 and ATP10A; and glucosylceramide for ATP10D (Naito et al., 2015; Roland et al., 2019; Shin and Takatsu, 2019; Takada et al., 2015; Takatsu et al., 2011, 2014). The other P4-ATPases (ATP8A1, ATP9A, ATP9B, ATP10B and ATP11B) primarily localize to intracellular compartments (Shin and Takatsu, 2019; Takatsu et al., 2011). We have previously demonstrated that the N-terminal and/or C-terminal cytoplasmic regions of P4-ATPases play crucial roles in their cellular localization (Okamoto et al., 2020; Takatsu et al., 2011). In particular, C-terminal splice variants of ATP11C exhibit distinct cellular localizations. For example, the C-terminal region of the ATP11C-a variant is crucial for its signal-dependent endocytosis via phosphorylation by PKCα, whereas the C-terminal region of the ATP11C-b variant allows its polarized localization on the plasma membrane (Takatsu et al., 2017; Takayama et al., 2019). However, the regulatory mechanism underlying ATP11C-b localization to the restricted plasma membrane region in polarized motile cells remain unknown.

Ezrin, radixin and moesin (collectively termed ERM proteins) are highly homologous actin-binding proteins of the FERM (4.1 and ERM) family, and link the actin cytoskeleton to the plasma membrane (Bretscher et al., 2002; Gautreau et al., 2002). ERM proteins thus regulate diverse biological processes, including cell migration/invasion, formation of microvilli, cell adhesion and membrane ruffling (Baumgartner et al., 2006; Clucas and Valderrama, 2014; Ivetic and Ridley, 2004; Lamb et al., 1997; Ng et al., 2001; Takeuchi et al., 1994; Tsukita and Yonemura, 1999; Valderrama et al., 2012). The ERM proteins comprised an N-terminal FERM domain, a C-terminal ERM association domain (C-ERMAD) and an α-helical region between these domains (Algrain et al., 1993; Gary and Bretscher, 1995; Turunen et al., 1994). The FERM domain interacts with integral membrane proteins localized to actin-rich plasma membrane regions, whereas the C-ERMAD contains F-actin-binding sites (Fehon et al., 2010). Owing to the intramolecular interaction between the FERM domain and C-ERMAD, the ERM proteins constitutively adopt a closed conformation, in which binding sites for membrane components and F-actin are masked (Pearson et al., 2000). However, upon phosphorylation of the C-terminal domain and/or phosphatidylinositol 4,5-bisphosphate binding to the FERM domain, the ERM proteins adopt an extended open conformation to expose protein-binding sites (Bretscher et al., 2002; Fievet et al., 2004; Hao et al., 2009; Simons et al., 1998).

We previously found that the ATP11C-b variant localizes to restricted regions of the plasma membrane in polarized cells (Takayama et al., 2019). In the present study, we sought to identify the regulatory mechanism underlying the ATP11C-b localization to restricted regions of the plasma membrane in polarized motile cells, which are as yet incompletely understood. We identified that ATP11C-b specifically interacts with ezrin, and demonstrated that this interaction is required for the polarized localization of ATP11C-b.

[1]Department of Physiological Chemistry, Graduate School of Pharmaceutical Sciences, Kyoto University, Sakyo-ku, Kyoto 606-8501, Japan. [2]Faculty of Pharmaceutical Sciences, Kyoto University, Sakyo-ku, Kyoto 606-8501, Japan.
*These authors contributed equally to this work

‡Author for correspondence (shin@pharm.kyoto-u.ac.jp)

H.I., 0000-0002-0137-7358; M.T., 0000-0002-7764-1610; H.-W.S., 0000-0002-9138-9554

Handling Editor: Jennifer Lippincott-Schwartz
Received 10 February 2021; Accepted 9 September 2021

Journal of Cell Science (2021) 134, jcs258523. doi:10.1242/jcs.258523

RESULTS

Crucial role for the LLxY motif in polarized plasma membrane localization of ATP11C-b

The *ATP11C* gene encodes three C-terminal splice variants: ATP11C-a, ATP11C-b and ATP11C-c (Fig. 1A) (Takayama et al., 2019). We previously demonstrated that ATP11C-b, but not ATP11C-a or ATP11C-c, exhibits polarized localization on the plasma membrane in highly motile breast cancer cells (MDA-MB-231) and in pro B cells (Ba/F3) (Takayama et al., 2019). Namely, ATP11C-b localization is restricted to the cell body region of the plasma membrane and excluded from membrane ruffles (Fig. 1Bb), whereas ATP11C-a is distributed throughout the plasma membrane with enrichment at membrane ruffles (Fig. 1Ba,C) (Takayama et al., 2019). Moreover, in polarized Ba/F3 cells, ATP11C-b is confined to the uropod in the cell posterior and is excluded from the cell anterior, including pseudopods (Fig. 1Db,E), while ATP11C-a is distributed throughout the plasma membrane (Fig. 1Da,E) (Takayama et al., 2019). We previously identified that the LLSYKH sequence in the ATP11C-b C-terminal region is sufficient for polarized localization of ATP11C-b (Takayama et al., 2019) (Fig. 1A). In the present study, we further confirmed that mutation of three amino acids, L1108, L1109 and Y1111 (Fig. 1A, bold), to alanine (3ala) caused mislocalization of ATP11C-b to membrane ruffles in MDA-MB-231 cells (Fig. 1Bc) and to the anterior of the cell in polarized Ba/F3 cells (Fig. 1Cc), indicating that the LLxY motif is crucial for the polarized localization of ATP11C-b.

We next determined whether redistribution of the ATP11C-b(3ala) mutant affected its flippase activity. We examined the flippase activities of cells stably expressing ATP11C-a, ATP11C-b(WT) or ATP11C-b(3ala) toward NBD-PS and NBD-PE, which are known substrates of ATP11C (Takada et al., 2015; Takatsu et al., 2014). Flippase activity of ATP11C-b(3ala) was comparable with that of ATP11C-b(WT) (Fig. S1A), and expression levels were comparable among ATP11C-a, ATP11C-b and ATP11C-b(3ala) (Fig. S1B). These results indicate that mislocalization did not affect its enzymatic activity. In addition, mislocalized ATP11C-b did not affect cell polarization, as lamellipodia and pseudopods were normally formed in MDA-MB-231 and Ba/F3 cells expressing ATP11C-b(3ala) (Fig. 1B,D, phalloidin panels).

Specific interaction of the ATP11C-b C-terminal region with ezrin

Next, we explored the mechanism underlying the confined localization of ATP11C-b. To this end, we performed yeast two-hybrid screening using the C-terminal region of ATP11C-b, ATP11C-b(CT), as a bait to identify proteins interacting with the ATP11C-b variant (Fig. 2A). Among the interacting candidates identified by the screening, ezrin was included. ATP11C-b(CT) but not ATP11C-a(CT) bound to ezrin (Fig. 2C), indicating an ATP11C-b-specific interaction. We also examined whether the other ERM proteins, radixin and moesin, interacted with ATP11C-b(CT) using a yeast two-hybrid assay, and found that, although ATP11C-b(CT) was able to interact with radixin and moesin, these interactions were much weaker than that with ezrin (Fig. 2D).

In the ERM proteins, the FERM domain binds C-ERMAD in the closed conformation. When the FERM domain is released from C-ERMAD, it binds the cytoplasmic regions of plasma membrane proteins, such as CD44, P-selectin glycoprotein ligand 1 (PSGL-1; also known as SELPLG), and intercellular adhesion molecules (ICAMs) (Mori et al., 2008; Serrador et al., 1997; Takai et al., 2007; Tsukita et al., 1994; Yonemura et al., 1998). The FERM domain can be divided into three subdomains, F1, F2 and F3 (Fig. 2B) (Phang et al., 2016). We determined which domain(s) of ezrin interacted with ATP11C-b(CT) (Fig. 2B,C). ATP11C-b(CT) interacted with the N-terminal FERM domain of ezrin but not with the C-terminal half (Fig. 2B,C). Moreover, ATP11C-b(CT) bound to ezrin-NT(1-206), indicating that the F1 and F2 subdomains were sufficient for interaction with ATP11C-b(CT) (Fig. 2B,C). Although neither full-length radixin nor moesin proteins robustly interacted with ATP11C-b(CT), their FERM domains interacted with ATP11C-b(CT) to a similar affinity to that of ezrin (Fig. 2D).

Subsequently, to determine which amino acid residues within ATP11C-b(CT) were required for its interaction with ezrin, we mutated multiple amino acids, including those crucial for polarized localization of ATP11C-b (L1108, L1109 and Y1111; Fig. 1). Mutation of L1108, L1109, Y1111 or K1112 to alanine, as well as the 3ala mutation almost completely abolished the interaction of ATP11C-b with ezrin in the two-hybrid assay (Fig. 2E). This indicated a correlation between the interaction of ATP11C-b with ezrin and its polarized localization.

We then confirmed the interaction between ATP11C-b(CT) and ezrin using a GST pull-down assay. When purified GST-fused ATP11C-a(CT), ATP11C-b(CT) or ATP11C-b(CT-3ala) prebound to glutathione magnetic beads were mixed with purified His6-fused full-length ezrin or its FERM domain, ATP11C-b(CT), but not ATP11C-b(CT-3ala) or ATP11C-a(CT), pulled down both ezrin constructs (Fig. 2F). When lysates prepared from cells expressing FLAG-tagged ezrin were mixed with the GST-fused ATP11C constructs, not only ezrin-FLAG (upper band) but also endogenous ezrin (lower band) were pulled down with ATP11C-b(CT), but not with ATP11C-b(CT-3ala) or ATP11C-a(CT) (Fig. 2G). These results demonstrate a direct and specific interaction of ATP11C-b(CT) with the ezrin FERM domain, and underscore the crucial role of the LLxY motif of ATP11C-b(CT) in this interaction.

Interaction and plasma membrane colocalization of a phosphomimetic ezrin mutant with ATP11C-b

The ERM proteins undergo an intramolecular interaction between the N-terminal FERM domain and C-ERMAD. In the closed conformation, the intramolecular interaction occlude binding sites for other proteins, such as membrane proteins and the actin cytoskeleton (Bretscher et al., 1995; Gary and Bretscher, 1995). Phosphorylation of a threonine residue in the C-ERMAD of the ERM proteins (T567 in ezrin, Fig. 2B) is crucial for ERM activation (Ivetic and Ridley, 2004). Upon phosphorylation and/or ligand binding, the resulting open conformation allows the ERM proteins to link between membrane proteins and the actin cytoskeleton (Simons et al., 1998).

To determine whether the open conformation of ezrin is required for its interaction with ATP11C-b, a phosphomimetic mutant [ezrin(T567D)] and nonphosphorylatable mutant [ezrin(T567A)] were subjected to the yeast two-hybrid assay. As shown in Fig. 2C, ezrin(T567D) but not ezrin(T567A), interacted with ATP11C-b(CT), indicating that ATP11C-b preferentially interacts with ezrin in its open conformation.

We then examined the localization of stably expressed, FLAG-tagged ezrin(WT), ezrin(T567D) and ezrin(T567A) in MDA-MB-231 cells (Fig. 3A), and those in MDA-MB-231 cells stably expressing HA-tagged ATP11C-b (Fig. 3C and Fig. S2F). Exogenously expressed ezrin(WT) and endogenous ezrin were distributed throughout the plasma membrane, with enrichment at phalloidin-positive lamellipodia in MDA-MB-231 cells (Fig. 3Aa, B and Fig. S2). Similarly, ezrin(T567A) was distributed throughout the plasma membrane, including in lamellipodia (Fig. 3Ac,B). By

Journal of Cell Science (2021) 134, jcs258523. doi:10.1242/jcs.258523

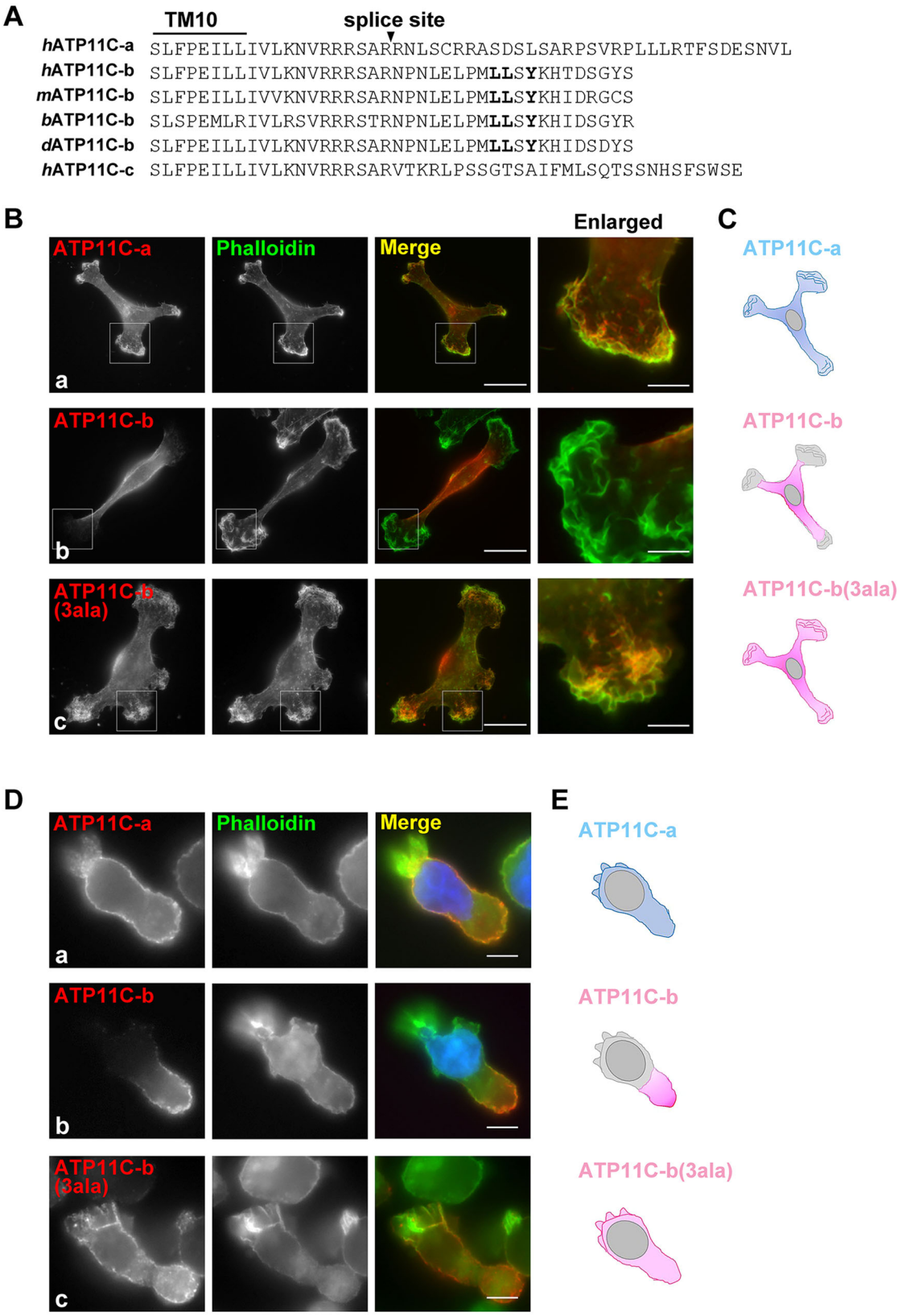

Fig. 1. The LLxY motif is crucial for polarized ATP11C-b localization. (A) Sequence alignments of C-terminal splice variants of ATP11C and mammalian variants of ATP11C-b. Leu1108, Leu1109 and Tyr1111 are indicated as bold letters. TM, transmembrane; h, human; m, mouse; r, rat; b, bovine; d, dog. (B) MDA-MB-231 cells and (D) Ba/F3 cells stably expressing C-terminally HA-tagged ATP11C-a, ATP11C-b or ATP11C-b(3ala), in which the Leu, Leu and Tyr residues shown by bold letters in A were substituted with Ala, fixed and incubated with anti-HA (3F10) antibody followed by incubation with Cy3-conjugated secondary antibody and Alexa488-conjugated phalloidin. Scale bars: 20 µm in B; 5 µm in D and higher magnification images in B. (C,E) Schematic illustrations of each ATP11C isoform and mutant localization. Light blue, ATP11C-a; pink, ATP11C-b.

Journal of Cell Science (2021) 134, jcs258523. doi:10.1242/jcs.258523

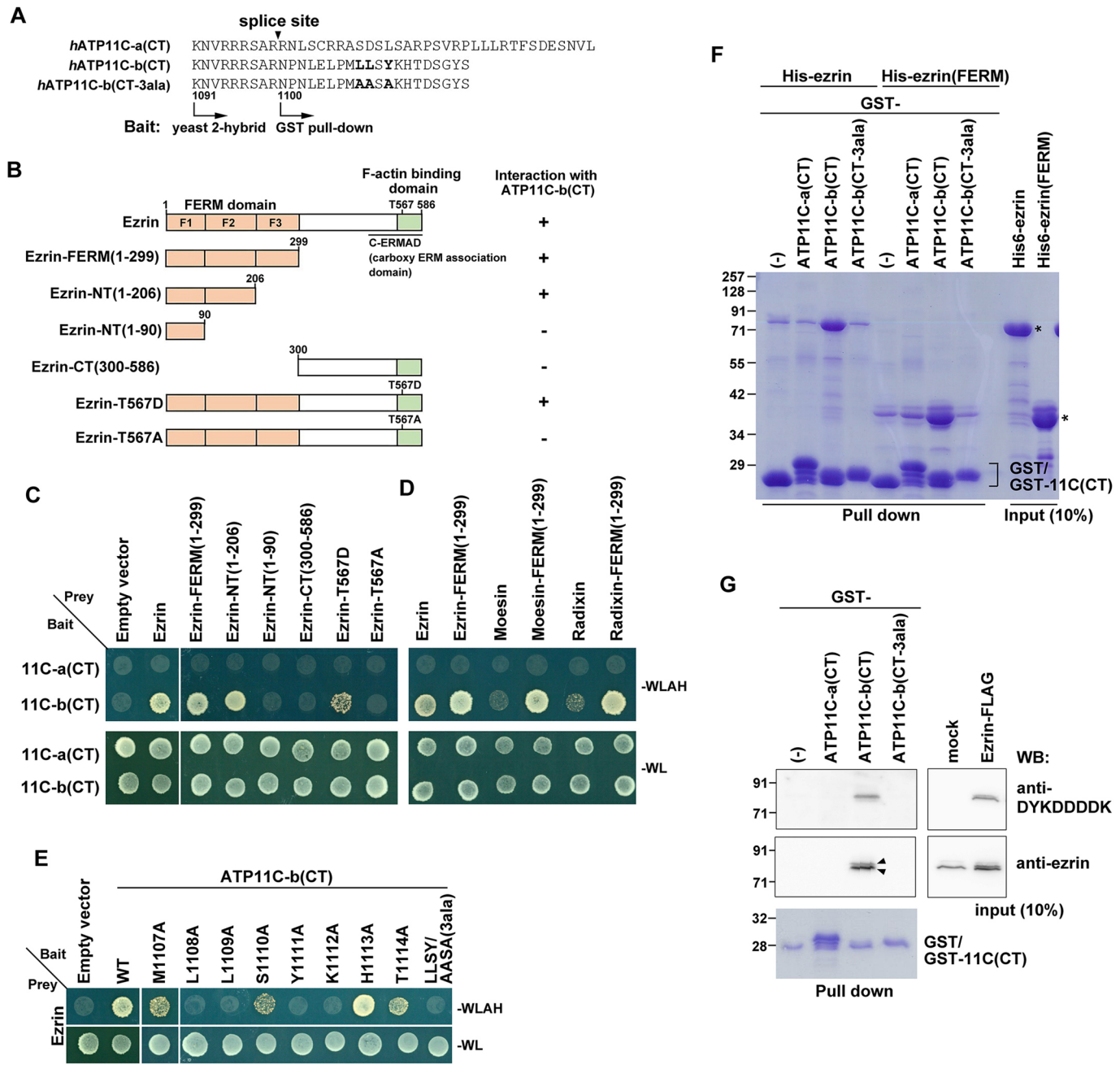

Fig. 2. Specific interaction between ATP11C-b and ezrin. (A) ATP11C-a(CT), ATP11C-b(CT) and ATP11C-b(CT-3ala) sequences for constructs used in yeast two-hybrid and GST pull-down analyses. (B) Schematic representation of the ezrin constructs used in the yeast two-hybrid assay. Summary of interactions between each ezrin mutant and ATP11C-b(CT) (right panel). (C,D) The ATP11C-a(CT) and ATP11C-b(CT) constructs shown in A were used as a bait in the two-hybrid assay. Various ERM constructs were used as prey, including: the full-length construct or FERM domains of ezrin, moesin and radixin; deletion mutants of ezrin shown in B; and full-length ezrin(T567D) and (T567A) mutants. AH109 yeast cells were transformed with the indicated bait and prey constructs, and transformants were grown in WLAH (Trp, Leu, Ade and His)- and WL-synthetic dropout medium, as specified. (E) AH109 yeast transformants expressing the indicated bait construct and ezrin prey construct were grown in WLAH- and WL-dropout medium, as specified. (F) Purified His6-tagged full-length ezrin or its FERM domain were pulled down with the indicated GST fusion protein [ATP11C-a(CT), ATP11C-b(CT) or ATP11C-b(CT-3ala), sequences shown in Fig. 2A] or GST alone (–). Bound materials were subjected to SDS-PAGE, and proteins were visualized by Coomassie Brilliant Blue staining. Asterisks indicate purified His-tagged proteins. (G) Lysates from HeLa cells transiently transfected with a FLAG-tagged ezrin construct were pulled down with the indicated GST fusion proteins. Bound proteins were subjected to SDS-PAGE and analyzed by immunoblotting with anti-DYKDDDDK or anti-ezrin antibodies. Endogenous ezrin (lower arrowhead) and exogenous ezrin-FLAG (upper arrowhead) are indicated. GST fusion proteins are stained with Coomassie Brilliant Blue.

contrast, ezrin(T567D) was localized exclusively to the cell body region of the plasma membrane and excluded from lamellipodia (Fig. 3Ab,B). The ezrin(T567D) signals were superimposed on that of ATP11C-b in the cell body region in cells co-expressing ezrin(T567D) and ATP11C-b (Fig. 3C). These observations indicate that ezrin in its open conformation localizes exclusively to cell body regions in which ATP11C-b is present.

We also stably expressed FLAG-tagged ezrin(WT), ezrin(T567D) or ezrin(T567A) in parental Ba/F3 cells (Fig. 3D) and in Ba/F3 cells stably expressing ATP11C-b-HA (Fig. 3F and

Journal of Cell Science (2021) 134, jcs258523. doi:10.1242/jcs.258523

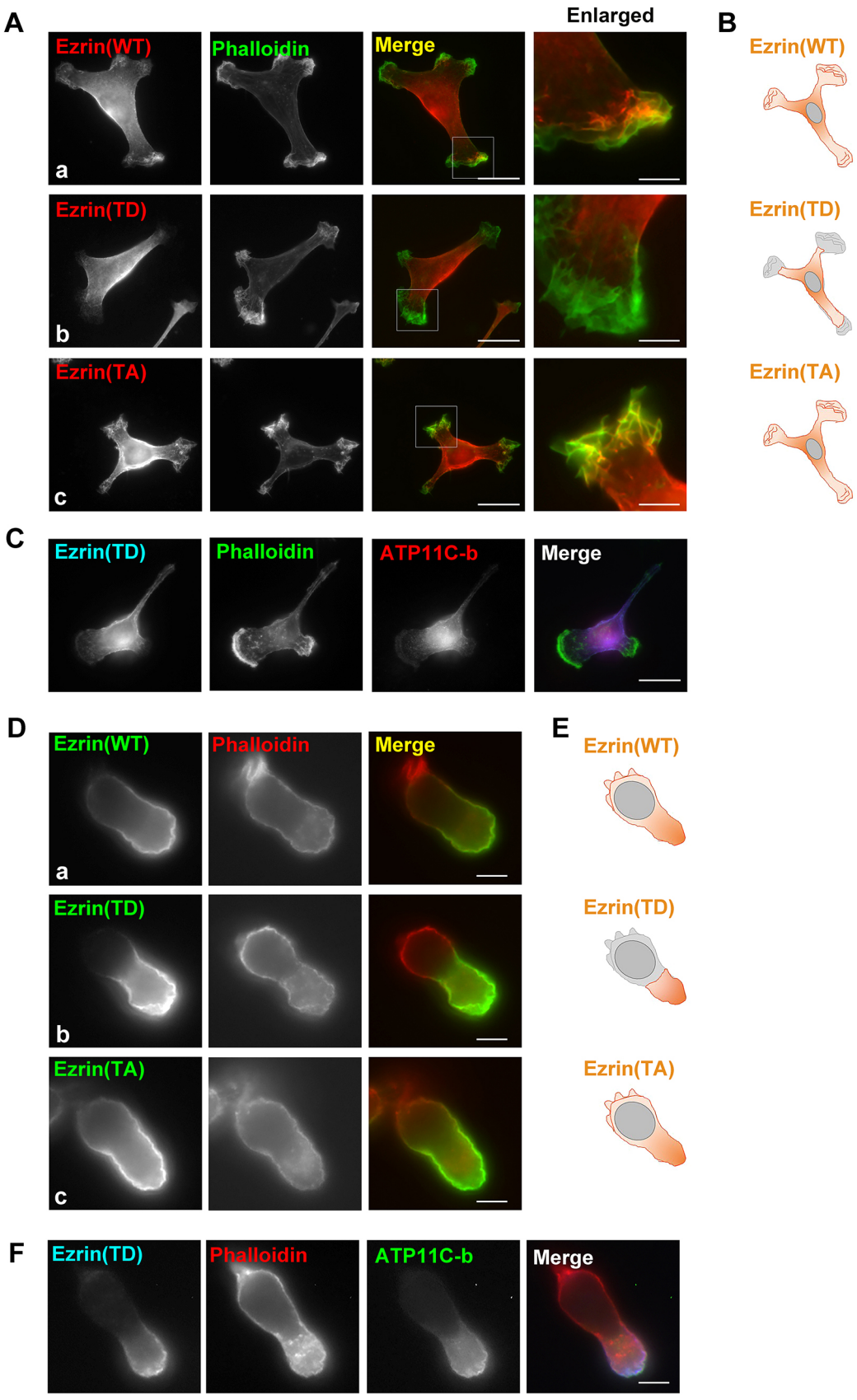

Fig. 3. See next page for legend.

Journal of Cell Science (2021) 134, jcs258523. doi:10.1242/jcs.258523

Fig. 3. Polarized localization of the phosphomimetic ezrin mutant in MDA-MB-231 and Ba/F3 cells. (A) MDA-MB-231 cells and (D) Ba/F3 cells stably expressing C-terminally FLAG-tagged ezrin(WT), ezrin(T567D) (TD) or ezrin(T567A) (TA) were fixed and stained for FLAG followed by incubation with Alexa555-conjugated anti-mouse secondary antibody and Alexa488-conjugated phalloidin (A) or Alexa488-conjugated anti-mouse secondary antibody and Alexa555-conjugated phalloidin (D). (C) MDA-MB-231 cells and (F) Ba/F3 cells stably co-expressing HA-tagged ATP11C-b and FLAG-tagged ezrin(T567D) were fixed and stained for HA and FLAG followed by incubation with Cy3-conjugated anti-rat and DyLight649-conjugated anti-mouse secondary antibodies, and Alexa488-conjugated phalloidin (C) or Alexa488-conjugated anti-rat and DyLight649-conjugated anti-mouse secondary antibody and Alexa555-conjugated phalloidin (F). (B,E) Schematic illustration of ezrin(WT) and each mutant localization presented in A and D. Scale bars: 20 µm (A,C); 5 µm (D,F, higher magnification images in A).

Fig. S2G). Exogenously expressed ezrin(WT) and ezrin(T567A) were distributed throughout the plasma membrane, with some enrichment at the uropod (Fig. 3Da,c,E). By contrast, ezrin(T567D) was exclusively localized to the uropod, where ATP11C-b localized (Fig. 3Db,E,F). We measured the fluorescence intensities of ezrin(WT) and ezrin(T567D) by line-scan from the back (uropod) to the front of Ba/F3 cells and quantified the ratio of the peak fluorescence intensity of the uropod to the cell front (Fig. S3A). The ratio for ezrin(T567D) was much larger than that for ezrin(WT), supporting that ezrin(T567D) predominantly localized to the uropod (Fig. S3B). These observations were consistent with previous reports showing that the phosphomimetic ezrin mutant is redistributed to the uropod of migrating T cells (Lee et al., 2004; Lorentzen et al., 2011; Martinelli et al., 2013; Serrador et al., 1997) and the ERM proteins are enriched at the rear of the cell in migrating melanoma cells and at the uropod of polarized T cells (Lorentzen et al., 2011; Serrador et al., 1997; Serrador et al., 2002). Taken together, these observations suggest that activated ezrin and ATP11C-b colocalized at the restricted region of the plasma membrane, and that this interaction could be required for the polarized localization of ATP11C-b.

Ezrin mutant expression does not affect ATP11C-b flippase activity

We next determined whether exogenous expression of ezrin mutants affected the enzymatic activity of ATP11C-b. When individual FLAG-tagged ezrin mutants were stably expressed in MDA-MB-231 cells and in MDA-MB-231 cells stably expressing ATP11C-b-HA, expression levels were comparable among the mutants, although the level of ezrin(WT) was slightly lower than the ezrin mutants (Fig. 4A). When flippase activities of NBD-PS and NBD-PE were examined in these cells, the activities were not significantly changed by exogenous expression of ezrin(WT) or its mutant in parental MDA-MB-231 cells or in MDA-MB-231 cells expressing ATP11C-b (Fig. 4B), indicating that exogenously expressed active ezrin did not affect ATP11C-b flippase activity at the plasma membrane.

The ERM proteins stabilize polarized ATP11C-b localization

Subsequently, we sought to determine whether ezrin is required for polarized ATP11C-b localization. To investigate this, we depleted ezrin alone or the three ERM proteins simultaneously using small interfering RNAs (siRNAs) in parental MDA-MB-231 cells (−) and MDA-MB-231 cells stably expressing either ATP11C-a or ATP11C-b. Efficient depletion of the ERM proteins was confirmed by immunoblot analysis (Fig. 5A). In cells stably expressing ATP11C-b-HA, depletion of ezrin alone or the ERM proteins promoted mislocalization of ATP11C-b to membrane ruffles (Fig. 5C). Approximately 13% of cells with depletion of ezrin alone exhibited ATP11C-b mislocalization, while 35% of cells with depletion of all ERMs exhibited ATP11C-b mislocalization (Fig. 5C,D). Contrastingly, ATP11C-a localization was not substantially affected by either ezrin or ERM depletion (Fig. 5B). These results indicate that ezrin primarily participates in stabilization of the polarized localization of ATP11C-b, although the other ERM proteins are also involved in ATP11C-b localization. Indeed, phosphomimetic radixin and moesin mutants also localized to the cell body region of the plasma membrane in MDA-MB-231 cells (Fig. S4A,B). It is notable that, as ezrin depletion decreased cell attachment to cover slips to some extent, ATP11C-b mislocalization could have been underestimated in ezrin-depleted cells.

We also examined flippase activities in ezrin-depleted or ERM-depleted cells. Endogenous flippase activities toward NBD-PS or NBD-PE or flippase activities promoted by exogenously expressed ATP11C-a or ATP11C-b were not significantly affected by either ezrin or ERM depletion, although the activities tended to be decreased in both ezrin-depleted and ERM-depleted cells (Fig. 5E). Although the reason for the decreasing trend of flippase activities is unknown, this could be due to decreased ATP11C protein levels in the depleted cells (Fig. 5A).

ATP11C-b stabilizes uropod localization of phosphorylated ERM proteins

Phosphorylated ERM (pERM) proteins can be visualized by antibodies specific to their phosphorylated threonine residues, and a prior study demonstrated that pERMs are localized to the uropod of T lymphocytes (Martinelli et al., 2013). Consistent with the study, we also found that pERM was concentrated at the uropod in some populations of polarized Ba/F3 cells (Fig. 6A (−)). We next sought to determine if ATP11C-b contributed to the polarized localization of pERM proteins by examining pERM localization in *Atp11c*-knockout cells, which we previously established using the CRISPR/Cas9 system (Takayama et al., 2019). In contrast to parental Ba/F3 cells, pERMs were redistributed to the leading edge in *Atp11c*-knockout cells (Fig. 6A). We visually assessed pERM enrichment at the uropod. Less than 10% of *Atp11c*-knockout cells exhibited pERM enrichment at the uropod, whereas over 30% of parental Ba/F3 cells exhibited this type of pERM localization (Fig. 6B). When HA-tagged ATP11C-a, ATP11C-b(WT), or ATP11C-b(3ala) was exogenously expressed in *Atp11c*-knockout cells, pERM enrichment to the uropod was restored by ATP11C-b(WT) but not by ATP11C-a or ATP11C-b(3ala) (Fig. 6). We also compared pERM fluorescence intensities by line-scan from the back (uropod) to the front of Ba/F3 cells (Fig. 6C) and quantified the ratio of the peak fluorescence intensity of the uropod to front (‘i/ii’ in Fig. 6C). The ratio was significantly decreased in *Atp11c*-knockout cells relative to control cells, indicating that the Atp11c depletion prevented pERM enrichment at the uropod. The peak intensity ratio was restored when ATP11C-b(WT), but not ATP11C-a or ATP11C-b(3ala), was expressed in *Atp11c*-knockout cells (Fig. 6D). The expression levels of the ATP11C-a, ATP11C-b(WT), and ATP11C-b(3ala) proteins were comparable, as revealed by immunoblot analysis (Fig. S5A). Flippase activities toward NBD-PS and NBD-PE were also comparable among those cells (Fig. S5B). Taken together, these findings demonstrate that ATP11C-b contributes to uropod localization of pERMs, including phosphorylated ezrin, via a direct interaction.

Journal of Cell Science (2021) 134, jcs258523. doi:10.1242/jcs.258523

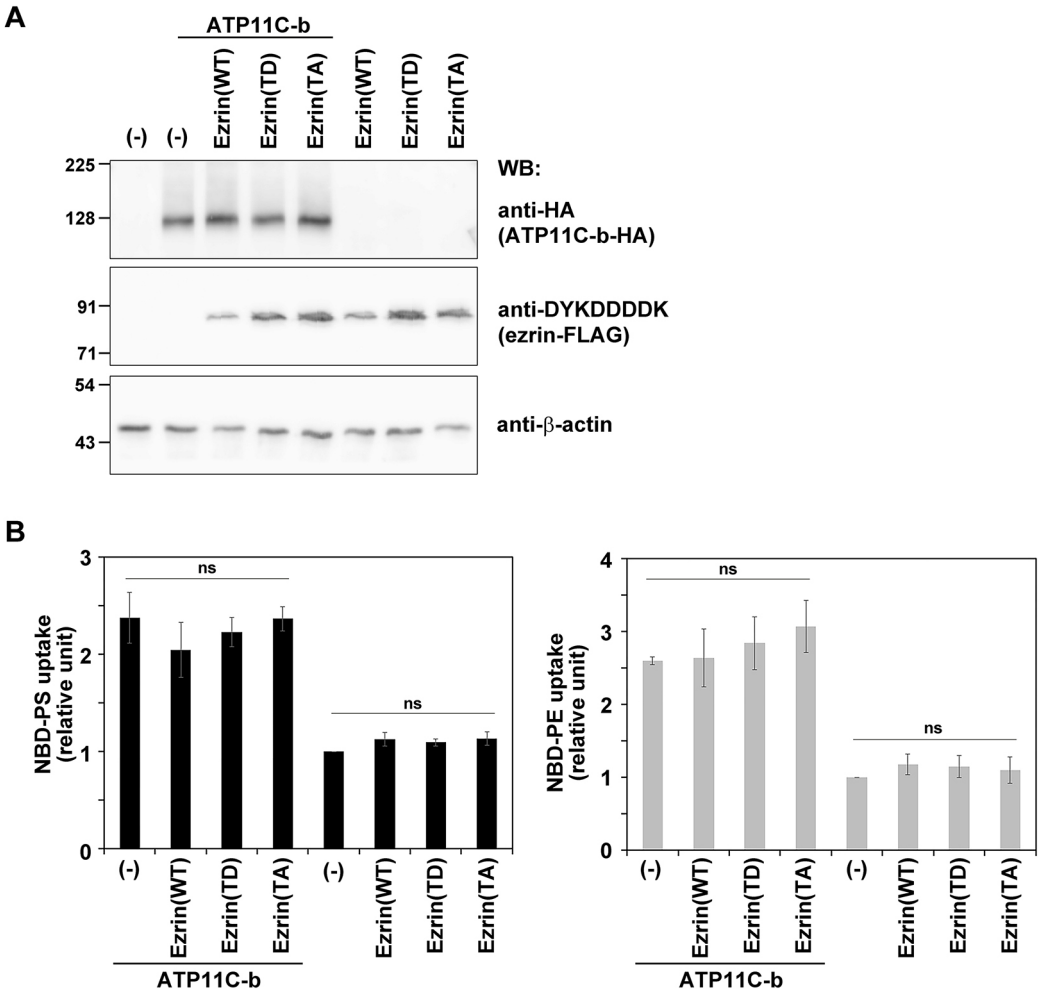

Fig. 4. Ezrin mutation did not affect ATP11C-b flippase activity. (A,B) Each FLAG-tagged ezrin was stably expressed in either MDA-MB-231 cells or MDA-MB-231 cells stably expressing HA-tagged ATP11C-b. (A) Lysates prepared from the cells described above were subjected to SDS-PAGE and immunoblotting using anti-HA, anti-DYKDDDDK or anti-β-actin (as an internal control) antibodies. (B) Cells were washed with flippase assay buffer and incubated for 5 min at 15°C with NBD-PS or for 15 min at 15°C with NBD-PE. After extraction with fatty acid-free BSA, the cellular fluorescence intensity was determined by flow cytometry. Uptake of NBD-conjugated lipids is shown relative to that in each control cell (−). Graphs display the average±s.d. from three (NBD-PS) or four (NBD-PE) independent experiments. A one-way ANOVA was performed to assess variance, and comparisons were made with Tukey's post-hoc analysis. Results are not significantly different (ns) in all cases.

ATP11C-b localizes to the MPA concentrated region

Phalloidin-positive F-actin is enriched in cell front structures such as membrane ruffles and pseudopods (Fig. 1, phalloidin panels and see Fig. 8) in migrating cells. Recently, membrane-proximal F-actin (MPA) density was visualized by a novel probe, MPAct, demonstrating that, in migrating cells, MPA density is high in the cell body and cell posterior, and low in the cell anterior (Bisaria et al., 2020) (Fig. S6). We expected that ATP11C-b would be localized to the MPA-enriched plasma membrane in MDA-MB-231 and Ba/F3 cells. To test this hypothesis, we expressed mRuby3-tagged MPAct in parental MDA-MB-231 (−) and Ba/F3 cells (−), and in the same cell lines stably expressing ATP11C-a, ATP11C-b or ATP11C-b(3ala) (Fig. 7). MPAct signals were concentrated much more robustly in the uropod than in pseudopods of parental Ba/F3 cells and Ba/F3 cells stably expressing each ATP11C (Fig. 7A), and in the cell body region than in the membrane ruffles of MDA-MB-231 cells and MDA-MB-231 cells stably expressing each ATP11C (Fig. 7B). We compared the fluorescence intensities of MPAct and phalloidin at the back and the front of Ba/F3 cells (Fig. S7). MPAct was enriched at the back (uropod) while phalloidin was greatly enriched at the front (pseudopods) of parental Ba/F3 cells. Moreover, MPAct signals were superimposed with ATP11C-b signals in the uropod and cell body regions (Fig. 7). These findings suggested that ATP11C-b is localized and stabilized in the MPA-enriched plasma membrane region via interacting with ezrin (Fig. 8). The polarized localization of MPAct and phalloidin signals was largely unaffected in *Atp11c*-knockout cells (Fig. S7), suggesting that ATP11C-b may not be necessary for the formation of the cell polarity, as was described previously (Takayama et al., 2019).

DISCUSSION

ATP11C-b exclusively localizes to the cell body region of the plasma membrane in motile MDA-MB-231 cells and to the uropod in polarized B lymphocytes (Takayama et al., 2019) (Fig. 7). Motile leukocytes exhibit polarized morphology characterized by formation of leading-edge pseudopods and a highly contractile uropod. Key regulatory components of uropod contractility include concentration of myosin II, actomyosin bundles and active Rho to the trailing edge (Heasman et al., 2010; Sánchez-Madrid and Serrador, 2009). Other uropod components include intercellular

Journal of Cell Science (2021) 134, jcs258523. doi:10.1242/jcs.258523

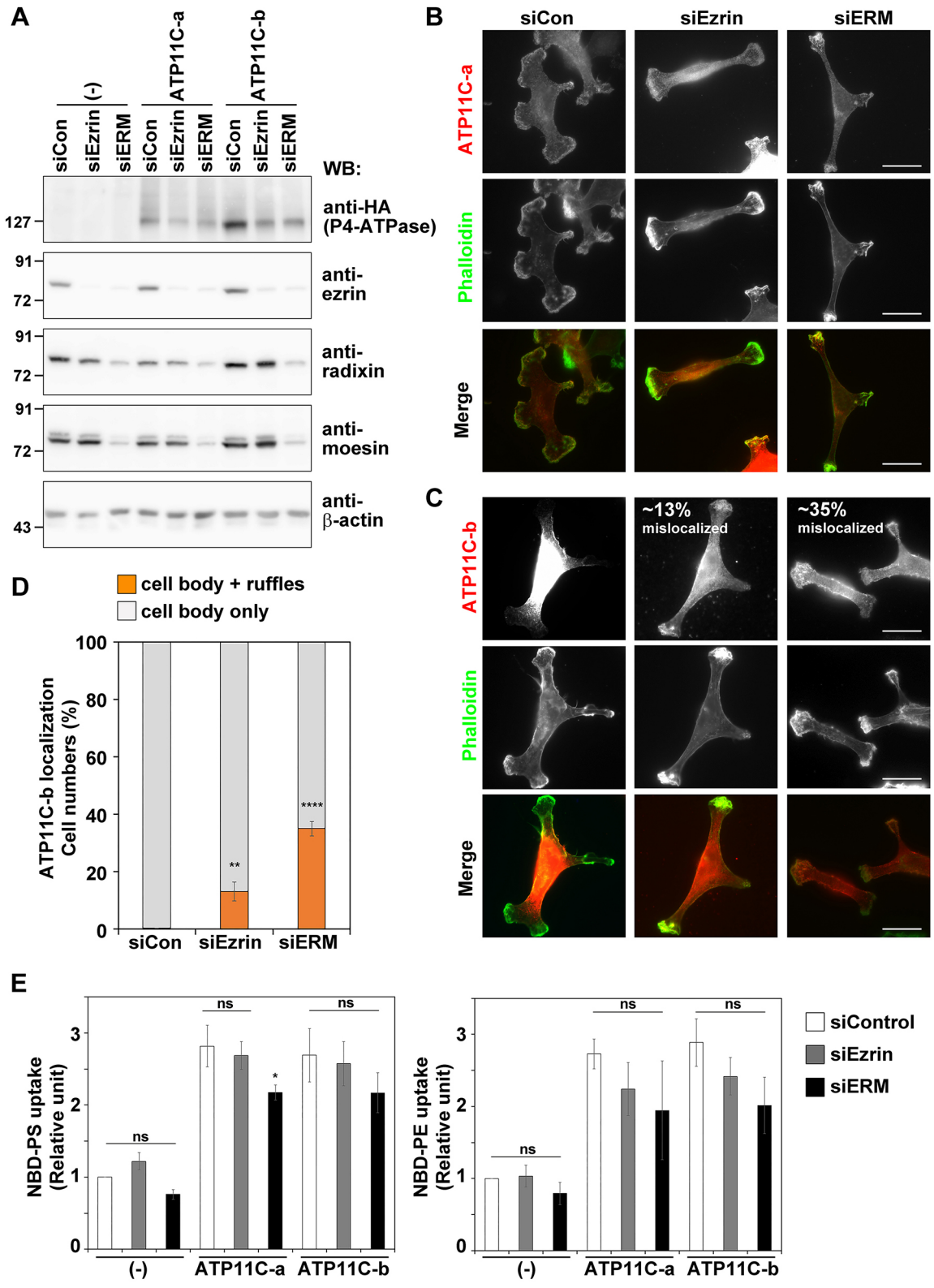

Fig. 5. See next page for legend.

adhesion molecules, such as PSGL-1, CD44 and ICAMs, which are actively targeted to the uropod through interaction of their juxtamembrane regions with ERM proteins (Alonso-Lebrero et al., 2000; Sánchez-Madrid and Serrador, 2009; Serrador et al., 1997; Serrador et al., 1998). Regulation of polarized leukocyte migration by the leading edge of migrating cells has been intensely investigated (Yang et al., 2016). The uropod has emerged as a crucial structure for proper leukocyte motility, which can also function as the driving center for polarization and migration (Hind et al., 2016; Lorentzen et al., 2011; Valignat et al., 2014). The ERM proteins contribute to neutrophil polarization by regulating Rac, RhoA and Cdc42 activities (Liu et al., 2015).

Fig. 5. Mislocalization of ATP11C-b in cells depleted of ezrin or ERM proteins. (A-E) MDA-MB-231 cells stably expressing ATP11C-a or ATP11C-b and parental cells were treated with a pool of siRNAs targeting ezrin alone; siRNAs targeting ezrin, radixin and moesin simultaneously (ERM); or non-targeting control siRNAs. siRNA-treated cells (A) were lysed for immunoblot analysis using antibodies to indicated proteins or (B,D) were fixed and immunostained for ATP11C using an anti-HA antibody followed by Cy3-conjugated anti-rat secondary antibody and incubated with Alexa488-conjugated phalloidin. (D) The number of cells in which ATP11C-b mislocalized to membrane ruffles or was excluded from membrane ruffles (cell body only) was counted and normalized to total counted cell numbers. Graphs display the average±s.d. from three independent experiments. Approximately 328-553 cells were counted for each sample. A one-way ANOVA was performed to assess variance, and comparisons were made with Tukey's post-hoc analysis. $^{**}P<0.01$, $^{****}P<0.0001$. (E) siRNA-treated cells were washed with flippase assay buffer and incubated for 5 min at 15°C with NBD-PS or 15 min at 15°C with NBD-PE. After extraction with fatty acid-free BSA, the residual fluorescence intensity associated with the cells was measured by flow cytometry. Uptake of NBD-tagged lipids relative to siCon-treated parental cells (−) is shown. Graphs display the average±s.d. from three independent experiments. A one-way ANOVA was performed to assess variance in D, and comparisons were made with Tukey's post-hoc analysis. $^{*}P<0.05$, not significant (ns). Scale bars: 20 µm.

In the present study, we identified ATP11C-b as an additional ERM-binding protein, demonstrating that this interaction occurred in the LLxY motif of its C-terminal cytoplasmic region. Interaction of ATP11C-b with ezrin appears to be dispensable for the enzymatic activity of ATP11C-b, as neither overexpression of ezrin and its constitutively active mutant [ezrin(T567D)] nor knockdown of ERM proteins significantly affected ATP11C-b enzymatic activity (Figs 5 and 6). By contrast, ezrin was required for proper polarized localization of ATP11C-b, as ATP11C-b was mislocalized to membrane ruffles of MDA-MB-231 cells depleted of ezrin or the ERM proteins (Fig. 5). The ATP11C-b(3ala) mutant was incapable of the polarized localization in both MDA-MB-231 and Ba/F3 cells, indicating the importance of the LLxY motif in targeting ATP11C-b to specialized regions of the plasma membrane. However, some proportion of ATP11C-b still exhibited polarized localization in the ezrin or ERM-knockdown cells. This could be due to incomplete depletion of ezrin or ERM proteins by the siRNAs and/or decreased cell adhesion and cell spreading in knockdown cells. Otherwise, an additional, unidentified interacting partner, which could bind to the LLxY motif, could participate in the recruitment of ATP11C-b to confined plasma membrane regions.

In migrating cells, phalloidin-positive F-actin is enriched at the leading edge, such as in membrane ruffles and pseudopods (Fig. 1, phalloidin panels and see Fig. 8). By contrast, membrane-proximal F-actin (MPA) visualized by the MPAct probe is concentrated in the cell body and cell posterior of migrating cells (Bisaria et al., 2020) (Fig. 7 and Fig. S7). F-actin, which is usually visualized by fluorescent phalloidin, is actively rearranged in the leading edge to form membrane ruffles and pseudopods, whereas MPA is instead concentrated in the cell posterior, and is known to prevent membrane protrusions (Bisaria et al., 2020). Moreover, a decrease in local ezrin abundance and dephosphorylation at the plasma membrane can initiate local membrane protrusions (Welf et al., 2020). Therefore, enrichment of active ezrin, MPA and ATP11C-b at the uropod and cell body could prevent membrane protrusions from these regions (Fig. 8).

Phosphorylated ERM proteins were shown to accumulate at the uropod of chemokine-stimulated T cells, and to contribute to uropod formation and cell polarization in cooperation with Rho signaling (Lee et al., 2004; Sánchez-Madrid and Serrador, 2009). With regard to the roles of the ERM proteins in T-cell polarization and migration, however, conflicting results have been reported. Some studies reported that expression of ezrin(T567D) increases the uropod size and promotes chemotaxis (Lee et al., 2004; Li et al., 2007; Martinelli et al., 2013), and T cells lacking ezrin show reduced chemotaxis (Chen et al., 2013). On the other hand, expression of constitutively active moesin(T558D) in T cells has been reported to delay chemokine-induced polarization (Brown et al., 2003), and T cells isolated from mice expressing ezrin(T567E) have been reported to exhibit decreased migration, which was attributed to increased membrane tension due to increased linkage between the actin cytoskeleton and membrane via ezrin(T567E) (Liu et al., 2012). In the present study, we showed that expression of ezrin(T567D) in Ba/F3 cells did not affect steady-state cell polarization. Moreover, *Atp11c*-knockout Ba/F3 cells did not exhibit considerable differences in steady-state cell polarization or migration relative to parental Ba/F3 cells (Fig. 6 and Fig. S7) (Takayama et al., 2019). Therefore, the interaction between phosphorylated ezrin and ATP11C-b is likely dispensable for steady-state cell polarization in this context.

By contrast, *Atp11c* ablation modestly but statistically significantly decreased uropod localization of pERMs, suggesting that polarized localization of phosphorylated ezrin could be stabilized and maintained at the uropod through its interaction with ATP11C-b. Because ERM proteins can interact with other uropod components, such as CD44 and PSGL-1 (Lee et al., 2004; Serrador et al., 2002), these plasma membrane proteins could also contribute to pERM stabilization at the uropod. A recent study revealed that ERM-binding proteins, such as PSGL-1 and CD44, retain their polarized localization to the uropod in neutrophils lacking ezrin and moesin (Panicker et al., 2020). It is therefore likely that cell polarization can be achieved through highly complex crosstalk among ERM proteins, plasma membrane proteins, the actin cytoskeleton and other signaling proteins, such as Rho family GTPases.

The physiological relevance of polarized ATP11C-b localization and its enzymatic activity at the restricted region of the plasma membrane remain to be elucidated. We speculate that PS is tightly confined to the cytosolic leaflet of the cell body and uropod, where ATP11C-b is localized, in migrating cells for the following reasons: (1) ATP11C is a major PS flippase in Ba/F3 cells (Fig. S2B) (Takayama et al., 2019); (2) ATP11C-a is downregulated by increased cytosolic Ca^{2+} concentration, whereas ATP11C-b is not affected by Ca^{2+} (Takatsu et al., 2017; Takayama et al., 2019); and (3) Ca^{2+} signaling via chemokine receptors and Ca^{2+} gradient between cell anterior and posterior are indispensable for cell migration (Wei et al., 2012). We postulate that transient PS exposure and recovery could be modulated by Ca^{2+} signaling and occur at the leading edge of migrating cells, where ATP11C-b is absent. Conversely, PS exposure is tightly prevented at the uropod, where ATP11C-b is present (Fig. 8). Thus, it is tempting to speculate that active PS-flip/flop contributes to membrane shape changes in pseudopods and membrane ruffles, while confinement of PS to the inner leaflet stabilizes the actin cytoskeleton, preventing membrane protrusions in the uropod and cell body during cell migration (Fig. 8). Although *Atp11c* depletion in Ba/F3 cells did not dramatically affect steady-state cell polarization and cell migration (Takayama et al., 2019), we cannot exclude the possibility that PS flipping activity contributes significantly to cell migration in cells activated by ligand stimulation rather than in the steady state. Another possibility is the contribution of PE flipping activity. Although PS flipping activity was mostly abolished in *Atp11c*-knockout cells, PE-flipping activity was reduced by ∼50% (Fig. S3). PE-flipping activity is required for cell polarity (Das

Journal of Cell Science (2021) 134, jcs258523. doi:10.1242/jcs.258523

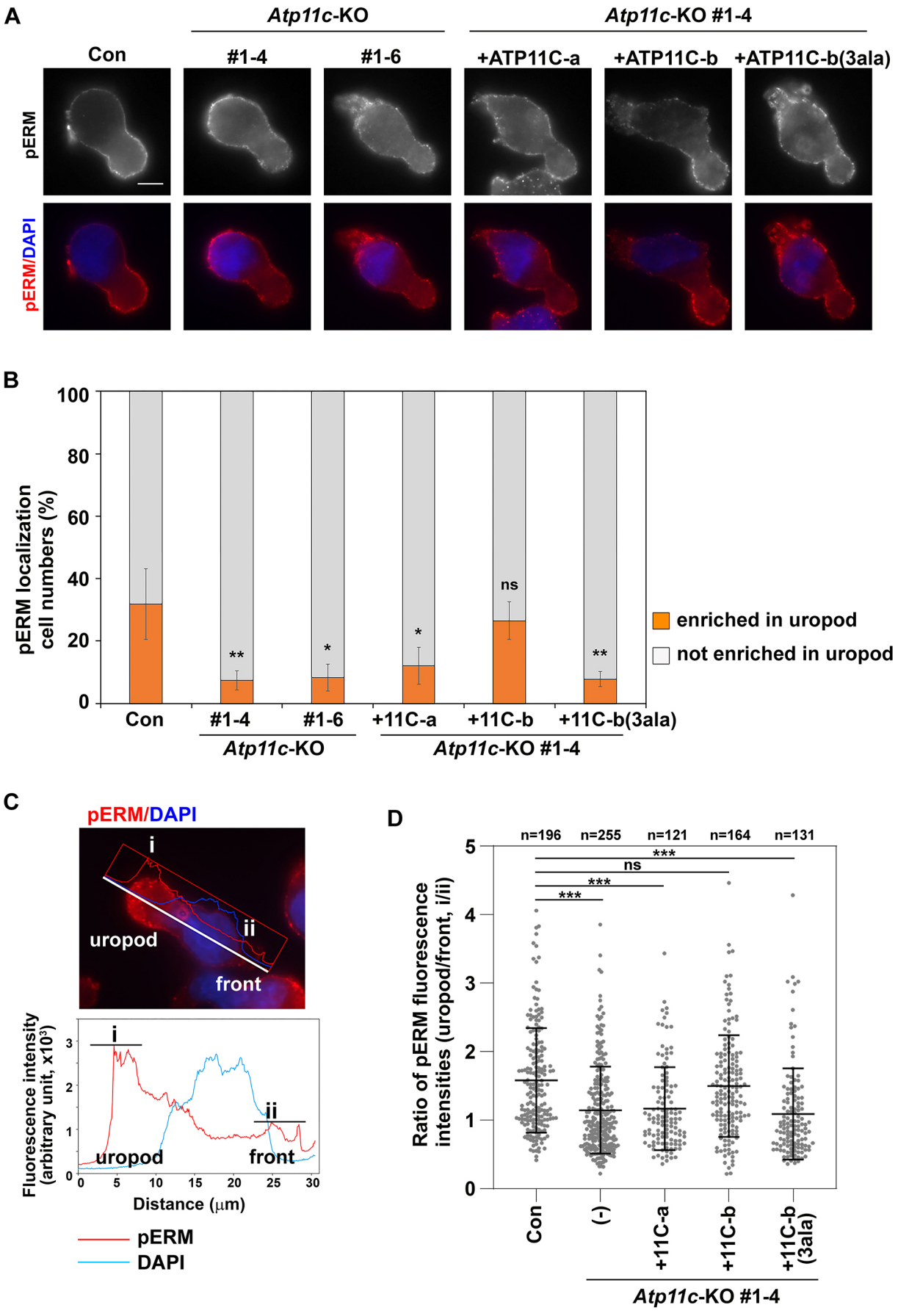

Fig. 6. See next page for legend.

Journal of Cell Science (2021) 134, jcs258523. doi:10.1242/jcs.258523

Fig. 6. Mislocalization of pERMs in *Atp11c*-knockout cells and rescue by ATP11C-b expression. (A) Parental Ba/F3 cells (Con), *Atp11c*-knockout cells and cells stably expressing CRISPR-resistant HA-tagged ATP11C-a, ATP11C-b or ATP11C-b(3ala) in the indicated *Atp11c*-knockout cell clone were fixed and immunostained using anti-pERM antibody followed by Alexa555-conjugated anti-mouse secondary antibody and incubated with DAPI. (B) Number of cells in which pERM is enriched in uropods (orange), and enriched in pseudopods and evenly distributed in uropods and pseudopods (light grey) was counted and normalized to total counted cell numbers. Graphs display the average±s.d. from three independent experiments. Approximately 203-329 cells were counted for each sample. A one-way ANOVA was performed to assess variance, and comparisons with parental cells (Con) were made with Dunnett's analysis. **P*<0.05, ***P*<0.01, not significant (ns). (C) A representative line-scan profile from the back (uropod) to the front of a Ba/F3 cell is shown. The line scan was performed using the ZEN software. (D) The ratio of the peak fluorescence intensity of the uropod to the front (i and ii in C) of pERM was calculated and expressed as scatter plots. Individual dots represent the ratios in individual cells. Graphs display the average ratio±s.d. from all analyzed cells. *n*=number of analyzed cells. A one-way ANOVA was performed to assess variance, and comparisons with parental cells (Con) were conducted using Dunnett's analysis. ****P*<0.0001; ns, not significant. Scale bar: 5 µm.

et al., 2012), is involved in cell migration (Kato et al., 2013) and plays a role in plasma membrane dynamics such as extracellular vesicle formation (Wehman et al., 2011), suggesting that the remaining PE flippase activity in *Atp11c*-knockout cells could participate in cell polarization and/or migration.

In the present study, we demonstrated that the ATP11C-b C-terminal region interacts with the F1 and F2 subdomains of the FERM domain via its LLxY motif. By contrast, previously identified ERM-binding proteins, such as ICAM-2, PSGL-1, CD44 and NHERF, interacted with the F3 subdomain (Hamada et al., 2003; Terawaki et al., 2006). The crystal structure of the radixin FERM domain complexed with the C-terminal peptide of ICAM-1 or NHERF-1 revealed that the F3 subdomain recognizes the RxxTYxVxxA or MDWxxx(L/I)Fxx(L/F) sequence motif, respectively. Moreover, sequences similar to the former motif were found in the cytoplasmic regions of other ERM-binding proteins, such as CD44, CD43, ICAM-1, ICAM-3 and PSGL-1 (Hamada et al., 2003; Terawaki et al., 2006). Considering that the LLxY motif is evolutionarily conserved in ATP11C-b of many other species and is crucial for the polarized localization ATP11C-b (Fig. 1A) (Takayama et al., 2019), the LLxY motif can be considered a novel ezrin-interacting motif.

MATERIALS AND METHODS

Plasmids

Expression vectors for C-terminally HA-tagged human P4-ATPases were constructed as previously described (Takatsu et al., 2014; Takayama et al., 2019). A partial cDNA encoding human ezrin (8-586 amino acids) was obtained by yeast two-hybrid screening. A cDNA encoding full-length ezrin was obtained by amplification using a sense primer including the sequence encoding the seven N-terminal amino acids of ezrin and an antisense primer. A cDNA encoding radixin was provided by RIKEN BRC through the National Bio-Resource Project of MEXT, Japan (Itoh et al., 2006; Kimura et al., 2006; Ota et al., 2004; Otsuki et al., 2005). cDNA encoding moesin (pHJ320) was provided by Addgene (plasmid #20671, deposited by Stephen Shaw; Hao et al., 2009). Truncation mutants of ezrin, radixin and moesin were constructed by PCR and EcoRI-XhoI digestion. To construct the amino acid-substituted ATP11C-b, ezrin mutants, and radixin and moesin mutants, each mutation was introduced into ATP11C-b cDNA, ezrin, radixin or moesin cDNA via PCR-based site-directed mutagenesis using the QuikChange II XL site-directed mutagenesis kit (Agilent Technologies) and/or the SLiCE cloning method (Zhang et al., 2012). To construct ATP11C-b(3ala), DNA fragments encoding the C-terminal region of ATP11C with the indicated mutations were synthesized and inserted to replace the same region of wild-type ATP11C cDNA as described previously (Takayama et al., 2019). Each mutation was confirmed by sequencing analysis. Expression vectors for C-terminal FLAG-tagged ezrin, radixin and moesin were constructed by inserting each cDNA (wild type or mutant) into pMXs-puro-FLAGc. For yeast two-hybrid analysis, each C-terminal fragment of ATP11C-a and ATP11C-b, and each ezrin mutant was amplified by PCR and inserted into pGBKT7 and pACT2 vectors, respectively. Full-length cDNA encoding radixin and moesin, and truncation mutants was amplified by PCR and inserted into a pACT2 vector. To construct N-terminally GST-tagged ATP11C(CT) and N-terminally His6-tagged ezrin and ezrin(FERM), amplified PCR products were inserted into pGEX-6P and pET-28 vectors, respectively. pLV-MPAct-mRuby3-IRES-Puro was a gift from Tobias Meyer (Addgene plasmid #155231). pMD2g/pRRE, pMD2.g and pRSV-Rev (Thomas et al., 2009) were kindly provided by Peter McPherson (McGill University, Canada).

Antibodies and reagents

Sources of antibodies used in the present study were as follows: monoclonal rabbit anti-radixin [EP1862Y; immunoblotting (WB) 1:500], Abcam; anti-pERM [48G2; immunofluorescence (IF), 1:500], Cell Signaling Technology; monoclonal mouse anti-ezrin (3C12; IF and WB, 1:500), anti-moesin (38/87; WB, 1:500) and anti-β-actin (C4; WB, 1:2000), all Santa Cruz Biotechnology; anti-β-tubulin (KMX-1; WB, 1:1000), Millipore; anti-DYKDDDDK (1E6; IF and WB, 1:500), Wako; monoclonal rat anti-HA (3F10; IF, 1:250; WB, 1:500), Roche Applied Science; and Alexa Fluor-conjugated secondary antibodies (1:500), Invitrogen; Cy3-, DyLight649-(1:500) and horseradish peroxidase-conjugated (1:3000) secondary antibodies, Jackson ImmunoResearch Laboratories. DAPI (1:10,000) and Alexa Fluor-conjugated phalloidin (1:500) were purchased from Molecular Probes. The NBD-labeled phospholipids (Avanti Polar Lipids) used were as follows: NBD-PS(1-oleyl-2-[6-[(7-nitro-2-1,3-benzoxadiazol-4-yl)amino]hexanoyl]-sn-glycero-3-phosphoserine), NBD-PE(1-oleyl-2-[6-[(7-nitro-2-1,3-benzoxadiazol-4-yl)amino]hexanoyl]-sn-glycero-3-phosphoethanolamine) and NBD-PC (1-oleyl-2-[6-[(7-nitro-2-1,3-benzoxadiazol-4-yl)amino]hexanoyl]-sn-glycero-3-phosphocholine).

Cell culture and establishment of stable cell lines

Ba/F3 cells (a kind gift from Shigekazu Nagata, Osaka University, Japan) and MDA-MB-231 cells were cultured per standard protocols. Cells expressing recombinant mouse interleukin 3 (IL3) were a kind gift from Shigekazu Nagata (Osaka University, Japan). Briefly, an IL3-dependent pro-B-cell line (Ba/F3) was maintained in RPMI-1640 medium containing 10% fetal calf serum (Gibco) (Fukunaga et al., 1990). MDA-MB-231 cells were cultured in Dulbecco's modified Eagle's medium (Nacalai Tesque) supplemented with 10% fetal calf serum (Gibco). Ba/F3 and MDA-MB-231 cells stably expressing each C-terminally HA-tagged ATP11C isoform and amino acid-substituted ATP11C-b, C-terminally FLAG-tagged ezrin, radixin and moesin, and amino acid-substituted ezrin, radixin and moesin were established as described previously (Takatsu et al., 2014; Takayama et al., 2019). To establish coexpressing cells, each C-terminally FLAG-tagged ezrin and its mutants were introduced in Ba/F3 and MDA-MB-231 cells stably expressing each C-terminally HA-tagged ATP11C isoform and mutant. For lentiviral production, pLV-MPAct-mRuby3-IRES-Puro was co-transfected with pMDLg/pRRE, pMD2.g and pRSV-Rev into HEK293T cells. The resultant lentiviruses were concentrated and used to infect Ba/F3 or MDA-MB-231 cells, or each ATP11C isoform-expressing cell as described previously (Takatsu et al., 2014). The infected cells were selected in medium containing puromycin (1 µg/ml).

Yeast two-hybrid analysis

Yeast transformation, two-hybrid screening and reporter assays were performed using the MATCHMAKER two-hybrid system (Clontech). AH109 yeast cells were transformed with pGBKT7-ATP11C-b(CT) using a lithium acetate-based method and grown on synthetic medium lacking tryptophan. The transformant was then transformed with a MATCHMAKER human leukocyte plasmid cDNA library (Clontech). Transformed cells were plated on synthetic medium lacking tryptophan, leucine, adenine and histidine. After 4 days, library plasmids from colonies

Journal of Cell Science (2021) 134, jcs258523. doi:10.1242/jcs.258523

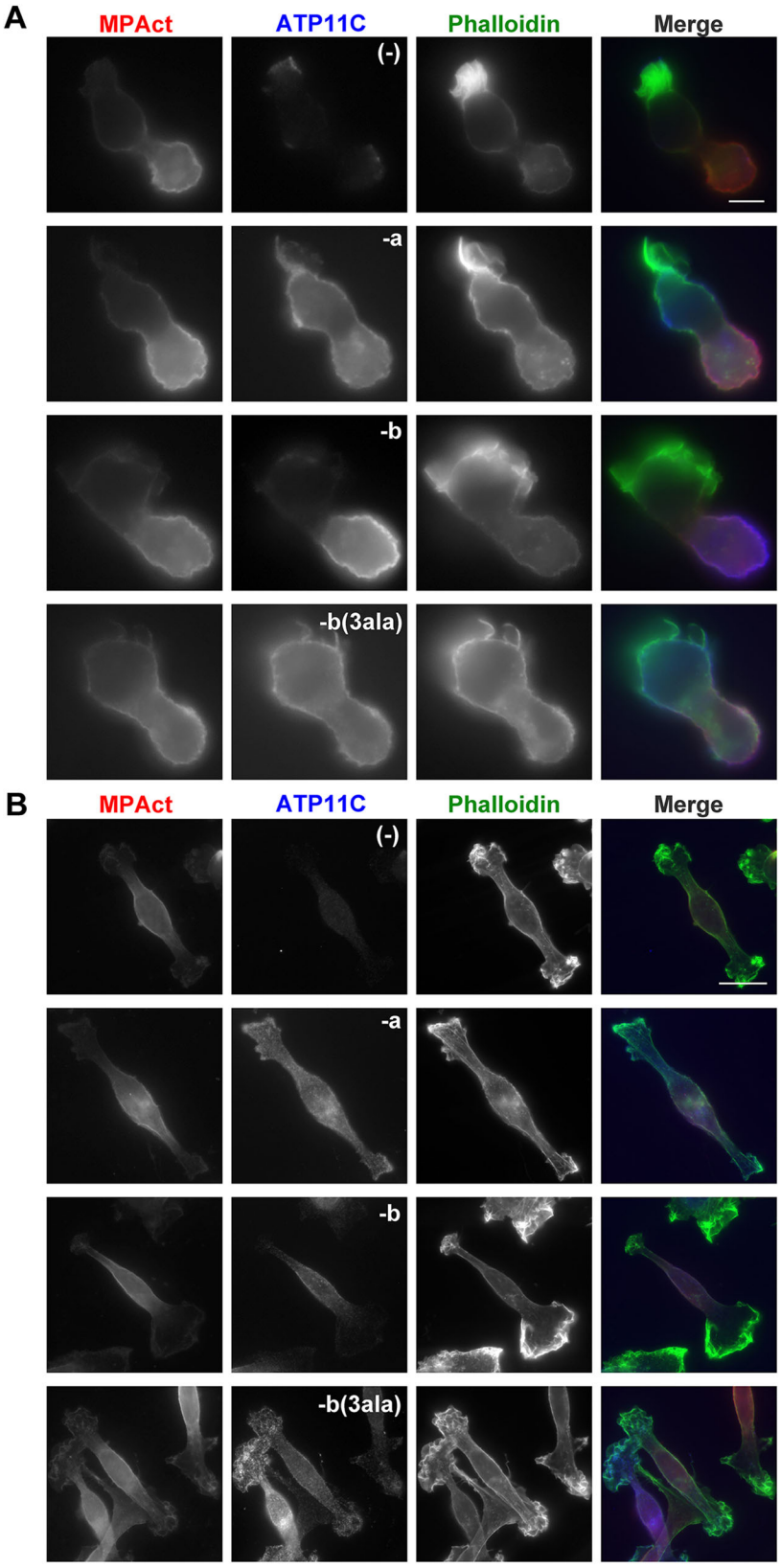

Fig. 7. ATP11C-b localizes to the MPA-enriched plasma membrane region. (A) Ba/F3 and (B) MDA-MB-231 cells expressing mRuby3-MPAct alone (–), or co-expressing mRuby3-MPAct and HA-tagged ATP11C-a, ATP11C-b or ATP11C-b(3ala) were fixed and stained for HA followed by incubation with Dylight649-conjugated anti-rat secondary antibody and Alexa488-conjugated phalloidin. Scale bars: 5 µm in A; 20 µm in B.

were rescued into HST08 *E. coli* cells by plating on ampicillin-containing medium. 1.9×10^6 colonies were screened. Out of 30 positive clones, one clone was for ezrin (8-586 amino acids). For interaction analysis, co-transformed AH109 cells with each bait and prey construct were plated on synthetic medium lacking tryptophan, leucine, adenine and histidine.

Recombinant protein purification

ATP11C-a(CT), ATP11C-b(CT) and ATP11C-b(CT-3ala) proteins fused to the C-terminus of glutathione *S*-transferase (GST) were expressed in *E. coli* BL-21-Codon Plus(DE3) (Stratagene) cells by treatment with 0.5 mM isopropyl-β-D-thiogalactopyranoside (Nacalai Tesque) overnight at 20°C.

Journal of Cell Science (2021) 134, jcs258523. doi:10.1242/jcs.258523

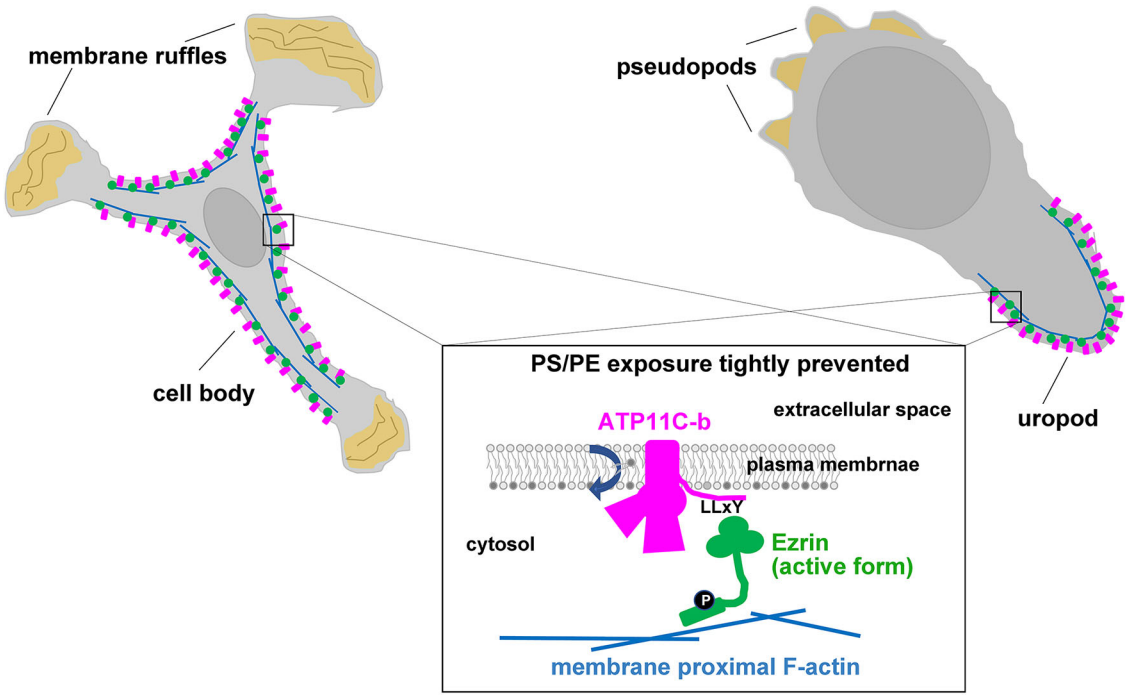

Fig. 8. Schematic model of ATP11C-b localization and interaction with ezrin in polarized cells. Phalloidin-positive F-actin, which is actively rearranged in membrane ruffles and pseudopods, is shown in yellow; membrane proximal F-actin, which is concentrated in cell body and uropod, is shown in blue.

Cells were harvested and resuspended in homogenization buffer [20 mM Tris-Cl (pH 8.0) and 300 mM NaCl] containing protease inhibitor cocktail (Wako) and homogenized by sonication. After addition of Triton X-100 (final concentration, 1%), homogenates were centrifuged to remove cell debris. The supernatant was incubated with paramagnetic glutathione-conjugated particles (MagneGST glutathione particles, Promega) for 2 h at 4°C. The magnetic beads were washed at least five times with homogenization buffer. Ezrin and ezrin(FERM) proteins fused to the C-terminus of 6xHis were expressed in *E. coli* BL-21-Codon Plus (DE3) (Stratagene) cells by treatment with 0.5 mM isopropyl-β-D-thiogalactopyranoside (Nacalai) overnight at 20°C. Cells were harvested and resuspended in homogenization buffer A [20 mM Tris-HCl (pH 8.0), 300 mM NaCl, 5 mM imidazole] containing protease inhibitor cocktail (Wako), and then homogenized by sonication. Homogenates were centrifuged to remove cell debris and the supernatant was incubated with COSMOGEL His-Accept resin (Nacalai Tesque) for 2 h at 4°C. Beads were washed at least five times with buffer B [20 mM Tris-HCl (pH 8.0), 300 mM NaCl and 20 mM imidazole] and proteins were eluted with buffer C [20 mM Tris-HCl (pH 8.0), 300 mM NaCl and 200 mM imidazole). Eluted proteins were used in a GST pull-down assay, which was performed in the presence of 150 mM imidazole to prevent non-specific binding.

GST pull-down assay

To prevent recombinant protein degradation and aggregation, the pull-down assay was performed with freshly prepared recombinant proteins. His6-tagged ezrin proteins were mixed with glutathione beads bearing each GST-fused protein prepared as described above in binding buffer [20 mM Tris-Cl (pH 7.5), 150 mM NaCl, 10% glycerol, 1% Triton X-100 and 150 mM imidazole] and incubated for 2 h at 4°C. MDA-MB-231 cells stably expressing FLAG-tagged ezrin were lysed in lysis buffer [20 mM Tris-Cl (pH 7.5), 150 mM NaCl, 1 mM EDTA and 1% Triton X-100] containing protease inhibitor cocktail (Wako) and phosphatase inhibitor cocktail (Wako). Cell lysates were mixed with glutathione beads bearing GST fusion proteins prepared as described above in binding buffer [20 mM Tris-Cl (pH 7.5), 150 mM NaCl, 10% glycerol and 1%Triton X-100] containing protease inhibitor cocktail and phosphatase inhibitor cocktail, and incubated for 2 h at 4°C. Beads were washed six times with binding buffer, and bound proteins were then eluted with SDS-PAGE sample buffer and subjected to western blot analysis. GST-fused proteins were separated by SDS-PAGE and visualized by Coomassie Brilliant Blue staining.

Immunofluorescence analysis

Immunostaining was performed as previously described (Shin et al., 2004; Takayama et al., 2019) and visualized using an Axiovert 200MAT microscope (Carl Zeiss). MDA-MB-231 cells seeded onto coverslips were fixed with 3% paraformaldehyde. To preserve the polarity of Ba/F3 cells, 3% PFA was added directly to cultured cells and incubated at room temperature for 30 min. Cells were then permeabilized with 0.2% saponin for 30 min or 0.1% Triton X-100 for 5 min at room temperature. We evaluated the polarized localization of pERM in Ba/F3 cells by both visual assessment and line-scan using the ZEN software (Carl Zeiss) to measure fluorescence intensities across the backs and fronts of cells. The ratio of the peak fluorescence intensity of the back to front was estimated. Polarized localization of ezrin(WT) and ezrin(T567D) mutant was also estimated by the ratio of the peak fluorescence intensity of the back to front. The fluorescence intensities of MPAct and phalloidin across the backs and fronts of Ba/F3 cells were analyzed by line-scan.

RNA interference

siRNAs targeting siEzrin, siRadixin and siMoesin, siGENOME SMARTpool (M017370, M011762 and M-011732, respectively) and siCon, non-targeting control siRNA pool #2 (D-001210), were purchased from Dharmacon. MDA-MB-231 cells stably expressing ATP11C-a or ATP11C-b were transfected with the siRNAs using Lipofectamine 3000 reagent (Invitrogen). Transfected cells were incubated for 72 h and processed for immunofluorescence and immunoblot analyses as described previously (Nakai et al., 2013; Shin et al., 2004; Tanaka et al., 2016).

Flippase assay

NBD-phospholipid incorporation was analyzed using flow cytometry as previously described (Takatsu et al., 2014) (Roland et al., 2019). In brief,

Ba/F3 cells were harvested from suspension culture by centrifugation. MDA-MB-231 cells were detached from dishes in PBS containing 5 mM EDTA and harvested by centrifugation. Cells (2×10^5 cells/sample) were washed and equilibrated at 15°C for 15 min in 100 µl Hank's balanced salt solution (pH 7.4) containing 1 g/l glucose (HBSS-glucose). An equal volume of 2 µM NBD-phospholipid in HBSS-glucose was added to the cell suspension and incubated at 15°C. At each time point, a 200 µl cell suspension was mixed with 200 µl ice-cold HBSS-glucose containing 5% fatty acid-free BSA (Wako) to extract NBD-lipids incorporated into the exoplasmic leaflet of the plasma membrane, as well as unincorporated lipids. Subsequently, the cells were analyzed with a FACSCalibur (BD Biosciences) to measure the fluorescence of NBD-lipids incorporated and translocated into the cytoplasmic leaflet of the plasma membrane (Fig. 4 and Fig. S1). Attached MDA-MB-231 cells were washed and equilibrated at 15°C for 15 min in 500 µl HBSS-glucose. The buffer was replaced with 1 µM NBD-phospholipid in HBSS-glucose and further incubated at 15°C. After incubation for the indicated times, the buffer was replaced with ice-cold PBS(−) containing 2.5% fatty acid-free BSA, 5 mM EDTA and 0.5 µg/ml propidium iodide (Nacalai Tesque), and cells were incubated on ice for 30 min. The detached cells were then analyzed with a FACSCalibur (BD Biosciences) (Fig. 5). Graphs for NBD-lipid flippase activities are expressed as averages±s.d. from at least three independent experiments.

Gene editing using the CRISPR/Cas9 system

The *Atp11c* gene was disrupted in Ba/F3 cells using the CRISPR/Cas9 system as described previously (Takayama et al., 2019). In the present study, we used two clones, #1-4 and #1-6 (Takayama et al., 2019), and used #1-4 for the rescue experiment. For the rescue experiment, CRISPR-resistant ATP11C-a and ATP11C-b were obtained by mutagenesis in the PAM sequences using a QuikChange II XL site-directed mutagenesis kit (Agilent Technologies). *Atp11c*-KO Ba/F3 cells (#1-4) stably expressing each C-terminally HA-tagged ATP11C isoform (CRISPR-resistant) and amino acid-substituted ATP11C-b(3ala) (CRISPR-resistant) were established as described previously (Takatsu et al., 2014).

Acknowledgements

We thank Toshio Kitamura (The University of Tokyo) and Hiroyuki Miyoshi (RIKEN BioResource Center) for providing plasmids for retroviral infection, and Sumio Sugano (The University of Tokyo) and Yoshihide Hayashizaki (RIKEN) for providing plasmids. We also thank Masato Kawasaki (KEK) for advice regarding protein tertiary structure.

Competing interests

The authors declare no competing or financial interests.

Author contributions

Conceptualization: H.T., H.-W.S.; Methodology: H.I., H.T.; Validation: H.I., H.T., A.H., M.T., R.N., Y.M., T.Y.; Formal analysis: H.I., H.T., A.H., H.-W.S.; Investigation: H.I., H.T., M.T., H.-W.S.; Resources: H.-W.S.; Data curation: H.I., H.T., A.H., H.-W.S.; Writing - original draft: H.-W.S.; Writing - review & editing: H.T., K.N., H.-W.S.; Visualization: H.I., H.T., A.H., M.T.; Supervision: H.-W.S.; Project administration: H.-W.S.; Funding acquisition: H.T., H.-W.S.

Funding

This work was supported by a Japan Society for the Promotion of Science KAKENHI (JP17H03655 and JP20H03209 to H.-W.S.; JP17K08270 and JP20K07325 to H.T.), by the Takeda Science Foundation (to H.-W.S.) and by the Uehara Memorial Foundation (to H.-W.S.).

Peer review history

The peer review history is available online at https://journals.biologists.com/jcs/article-lookup/doi/10.1242/jcs.258523.

References

Algrain, M., Turunen, O., Vaheri, A., Louvard, D. and Arpin, M. (1993). Ezrin contains cytoskeleton and membrane binding domains accounting for its proposed role as a membrane-cytoskeletal linker. *J. Cell Biol.* **120**, 129-139. doi:10.1083/jcb.120.1.129

Alonso-Lebrero, J. L., Serrador, J. M., Dominguez-Jiménez, C., Barreiro, O., Luque, A., del Pozo, M. A., Snapp, K., Kansas, G., Schwartz-Albiez, R., Furthmayr, H. et al. (2000). Polarization and interaction of adhesion molecules P-selectin glycoprotein ligand 1 and intercellular adhesion molecule 3 with moesin and ezrin in myeloid cells. *Blood* **95**, 2413-2419. doi:10.1182/blood.V95.7.2413

Andersen, J. P., Vestergaard, A. L., Mikkelsen, S. A., Mogensen, L. S., Chalat, M. and Molday, R. S. (2016). P4-ATPases as phospholipid flippases-structure, function, and enigmas. *Front. Physiol.* **7**, 275. doi:10.3389/fphys.2016.00275

Baumgartner, M., Sillman, A. L., Blackwood, E. M., Srivastava, J., Madson, N., Schilling, J. W., Wright, J. H. and Barber, D. L. (2006). The Nck-interacting kinase phosphorylates ERM proteins for formation of lamellipodium by growth factors. *Proc. Natl. Acad. Sci. USA* **103**, 13391-13396. doi:10.1073/pnas.0605950103

Bevers, E. M. and Williamson, P. L. (2016). Getting to the outer leaflet: physiology of phosphatidylserine exposure at the plasma membrane. *Physiol. Rev.* **96**, 605-645. doi:10.1152/physrev.00020.2015

Bisaria, A., Hayer, A., Garbett, D., Cohen, D. and Meyer, T. (2020). Membrane-proximal F-actin restricts local membrane protrusions and directs cell migration. *Science* **368**, 1205-1210. doi:10.1126/science.aay7794

Bretscher, A., Gary, R. and Berryman, M. (1995). Soluble ezrin purified from placenta exists as stable monomers and elongated dimers with masked C-terminal ezrin-radixin-moesin association domains. *Biochemistry* **34**, 16830-16837. doi:10.1021/bi00051a034

Bretscher, A., Edwards, K. and Fehon, R. G. (2002). ERM proteins and merlin: integrators at the cell cortex. *Nat. Rev. Mol. Cell Biol.* **3**, 586-599. doi:10.1038/nrm882

Brown, M. J., Nijhara, R., Hallam, J. A., Gignac, M., Yamada, K. M., Erlandsen, S. L., Delon, J., Kruhlak, M. and Shaw, S. (2003). Chemokine stimulation of human peripheral blood T lymphocytes induces rapid dephosphorylation of ERM proteins, which facilitates loss of microvilli and polarization. *Blood* **102**, 3890-3899. doi:10.1182/blood-2002-12-3807

Chen, E. J. H., Shaffer, M. H., Williamson, E. K., Huang, Y. and Burkhardt, J. K. (2013). Ezrin and moesin are required for efficient T cell adhesion and homing to lymphoid organs. *PLoS ONE* **8**, e52368. doi:10.1371/journal.pone.0052368

Clucas, J. and Valderrama, F. (2014). ERM proteins in cancer progression. *J. Cell Sci.* **127**, 267-275. doi:10.1242/jcs.133108

Coleman, J. A., Quazi, F. and Molday, R. S. (2013). Mammalian P4-ATPases and ABC transporters and their role in phospholipid transport. *Biochim. Biophys. Acta Mol. Cell Biol. Lipids* **1831**, 555-574. doi:10.1016/j.bbalip.2012.10.006

Das, A., Slaughter, B. D., Unruh, J. R., Bradford, W. D., Alexander, R., Rubinstein, B. and Li, R. (2012). Flippase-mediated phospholipid asymmetry promotes fast Cdc42 recycling in dynamic maintenance of cell polarity. *Nat. Cell Biol.* **14**, 304-310. doi:10.1038/ncb2444

Fehon, R. G., McClatchey, A. I. and Bretscher, A. (2010). Organizing the cell cortex: the role of ERM proteins. *Nat. Rev. Mol. Cell Biol.* **11**, 276-287. doi:10.1038/nrm2866

Fievet, B. T., Gautreau, A., Roy, C., Del Maestro, L., Mangeat, P., Louvard, D. and Arpin, M. (2004). Phosphoinositide binding and phosphorylation act sequentially in the activation mechanism of ezrin. *J. Cell Biol.* **164**, 653-659. doi:10.1083/jcb.200307032

Fukunaga, R., Ishizaka-Ikeda, E. and Nagata, S. (1990). Purification and characterization of the receptor for murine granulocyte colony-stimulating factor. *J. Biol. Chem.* **265**, 14008-14015. doi:10.1016/S0021-9258(18)77449-8

Gary, R. and Bretscher, A. (1995). Ezrin self-association involves binding of an N-terminal domain to a normally masked C-terminal domain that includes the F-actin binding site. *Mol. Biol. Cell* **6**, 1061-1075. doi:10.1091/mbc.6.8.1061

Gautreau, A., Louvard, D. and Arpin, M. (2002). ERM proteins and NF2 tumor suppressor: the Yin and Yang of cortical actin organization and cell growth signaling. *Curr. Opin. Cell Biol.* **14**, 104-109. doi:10.1016/S0955-0674(01)00300-3

Hamada, K., Shimizu, T., Yonemura, S., Tsukita, S., Tsukita, S. and Hakoshima, T. (2003). Structural basis of adhesion-molecule recognition by ERM proteins revealed by the crystal structure of the radixin-ICAM-2 complex. *EMBO J.* **22**, 502-514. doi:10.1093/emboj/cdg039

Hao, J.-J., Liu, Y., Kruhlak, M., Debell, K. E., Rellahan, B. L. and Shaw, S. (2009). Phospholipase C-mediated hydrolysis of PIP2 releases ERM proteins from lymphocyte membrane. *J. Cell Biol.* **184**, 451-462. doi:10.1083/jcb.200807047

Heasman, S. J., Carlin, L. M., Cox, S., Ng, T. and Ridley, A. J. (2010). Coordinated RhoA signaling at the leading edge and uropod is required for T cell transendothelial migration. *J. Cell Biol.* **190**, 553-563. doi:10.1083/jcb.201002067

Hind, L. E., Vincent, W. J. B. and Huttenlocher, A. (2016). Leading from the back: the role of the uropod in neutrophil polarization and migration. *Dev. Cell* **38**, 161-169. doi:10.1016/j.devcel.2016.06.031

Itoh, M., Yasunishi, A., Imamura, K., Kanamori-Katayama, M., Suzuki, H., Suzuki, M., Carninci, P., Kawai, J. and Hayashizaki, Y. (2006). Constructing ORFeome resources with removable termination codons. *BioTechniques* **41**, 44-50. doi:10.2144/000112209

Ivetic, A. and Ridley, A. J. (2004). Ezrin/radixin/moesin proteins and Rho GTPase signalling in leucocytes. *Immunology* **112**, 165-176. doi:10.1111/j.1365-2567.2004.01882.x

Kato, U., Inadome, H., Yamamoto, M., Emoto, K., Kobayashi, T. and Umeda, M. (2013). Role for phospholipid flippase complex of ATP8A1 and CDC50A proteins in cell migration. *J. Biol. Chem.* **288**, 4922-4934. doi:10.1074/jbc.M112.402701

Kimura, K., Wakamatsu, A., Suzuki, Y., Ota, T., Nishikawa, T., Yamashita, R., Yamamoto, J., Sekine, M., Tsuritani, K., Wakaguri, H. et al. (2006). Diversification of transcriptional modulation: large-scale identification and characterization of putative alternative promoters of human genes. *Genome Res.* **16**, 55-65. doi:10.1101/gr.4039406

Lamb, R. F., Ozanne, B. W., Roy, C., McGarry, L., Stipp, C., Mangeat, P. and Jay, D. G. (1997). Essential functions of ezrin in maintenance of cell shape and lamellipodial extension in normal and transformed fibroblasts. *Curr. Biol.* **7**, 682-688. doi:10.1016/S0960-9822(06)00295-8

Lee, J.-H., Katakai, T., Hara, T., Gonda, H., Sugai, M. and Shimizu, A. (2004). Roles of p-ERM and Rho-ROCK signaling in lymphocyte polarity and uropod formation. *J. Cell Biol.* **167**, 327-337. doi:10.1083/jcb.200403091

Li, Y., Harada, T., Juang, Y.-T., Kyttaris, V. C., Wang, Y., Zidanic, M., Tung, K. and Tsokos, G. C. (2007). Phosphorylated ERM is responsible for increased T cell polarization, adhesion, and migration in patients with systemic lupus erythematosus. *J. Immunol.* **178**, 1938-1947. doi:10.4049/jimmunol.178.3.1938

Liu, Y., Belkina, N. V., Park, C., Nambiar, R., Loughhead, S. M., Patino-Lopez, G., Ben-Aissa, K., Hao, J.-J., Kruhlak, M. J., Qi, H. et al. (2012). Constitutively active ezrin increases membrane tension, slows migration, and impedes endothelial transmigration of lymphocytes in vivo in mice. *Blood* **119**, 445-453. doi:10.1182/blood-2011-07-368860

Liu, X., Yang, T., Suzuki, K., Tsukita, S., Ishii, M., Zhou, S., Wang, G., Cao, L., Qian, F., Taylor, S. et al. (2015). Moesin and myosin phosphatase confine neutrophil orientation in a chemotactic gradient. *J. Exp. Med.* **212**, 267-280. doi:10.1084/jem.20140508

Lorentzen, A., Bamber, J., Sadok, A., Elson-Schwab, I. and Marshall, C. J. (2011). An ezrin-rich, rigid uropod-like structure directs movement of amoeboid blebbing cells. *J. Cell Sci.* **124**, 1256-1267. doi:10.1242/jcs.074849

Martinelli, S., Chen, E. J. H., Clarke, F., Lyck, R., Affentranger, S., Burkhardt, J. K. and Niggli, V. (2013). Ezrin/Radixin/Moesin proteins and flotillins cooperate to promote uropod formation in T cells. *Front. Immunol.* **4**, 84. doi:10.3389/fimmu.2013.00084

Mori, T., Kitano, K., Terawaki, S., Maesaki, R., Fukami, Y. and Hakoshima, T. (2008). Structural basis for CD44 recognition by ERM proteins. *J. Biol. Chem.* **283**, 29602-29612. doi:10.1074/jbc.M803606200

Murate, M., Abe, M., Kasahara, K., Iwabuchi, K., Umeda, M. and Kobayashi, T. (2015). Transbilayer distribution of lipids at nano scale. *J. Cell Sci.* **128**, 1627-1638.

Naito, T., Takatsu, H., Miyano, R., Takada, N., Nakayama, K. and Shin, H.-W. (2015). Phospholipid Flippase ATP10A translocates phosphatidylcholine and is involved in plasma membrane dynamics. *J. Biol. Chem.* **290**, 15004-15017. doi:10.1074/jbc.M115.655191

Nakai, W., Kondo, Y., Saitoh, A., Naito, T., Nakayama, K. and Shin, H.-W. (2013). ARF1 and ARF4 regulate recycling endosomal morphology and retrograde transport from endosomes to the Golgi apparatus. *Mol. Biol. Cell* **24**, 2570-2581. doi:10.1091/mbc.e13-04-0197

Ng, T., Parsons, M., Hughes, W. E., Monypenny, J., Zicha, D., Gautreau, A., Arpin, M., Gschmeissner, S., Verveer, P. J., Bastiaens, P. I. et al. (2001). Ezrin is a downstream effector of trafficking PKC-integrin complexes involved in the control of cell motility. *EMBO J.* **20**, 2723-2741. doi:10.1093/emboj/20.11.2723

Okamoto, S., Naito, T., Shigetomi, R., Kosugi, Y., Nakayama, K., Takatsu, H. and Shin, H.-W. (2020). The N- or C-terminal cytoplasmic regions of P4-ATPases determine their cellular localization. *Mol. Biol. Cell* **31**, 2115-2124. doi:10.1091/mbc.E20-04-0225

Ota, T., Suzuki, Y., Nishikawa, T., Otsuki, T., Sugiyama, T., Irie, R., Wakamatsu, A., Hayashi, K., Sato, H., Nagai, K., et al. (2004). Complete sequencing and characterization of 21,243 full-length human cDNAs. *Nat. Genet.* **36**, 40-45. doi:10.1038/ng1285

Otsuki, T., Ota, T., Nishikawa, T., Hayashi, K., Suzuki, Y., Yamamoto, J.-I., Wakamatsu, A., Kimura, K., Sakamoto, K., Hatano, N. et al. (2005). Signal sequence and keyword trap in silico for selection of full-length human cDNAs encoding secretion or membrane proteins from oligo-capped cDNA libraries. *DNA Res.* **12**, 117-126. doi:10.1093/dnares/12.2.117

Palmgren, M. G. and Nissen, P. (2011). P-type ATPases. *Annu. Rev. Biophys.* **40**, 243-266. doi:10.1146/annurev.biophys.093008.131331

Palmgren, M., Østerberg, J. T., Nintemann, S. J., Poulsen, L. R. and López-Marqués, R. L. (2019). Evolution and a revised nomenclature of P4 ATPases, a eukaryotic family of lipid flippases. *Biochim. Biophys. Acta Biomembr.* **1861**, 1135-1151. doi:10.1016/j.bbamem.2019.02.006

Panicker, S. R., Yago, T., Shao, B. and McEver, R. P. (2020). Neutrophils lacking ERM proteins polarize and crawl directionally but have decreased adhesion strength. *Blood Adv.* **4**, 3559-3571. doi:10.1182/bloodadvances.2020002423

Pearson, M. A., Reczek, D., Bretscher, A. and Karplus, P. A. (2000). Structure of the ERM protein moesin reveals the FERM domain fold masked by an extended actin binding tail domain. *Cell* **101**, 259-270. doi:10.1016/S0092-8674(00)80836-3

Phang, J. M., Harrop, S. J., Duff, A. P., Sokolova, A. V., Crossett, B., Walsh, J. C., Beckham, S. A., Nguyen, C. D., Davies, R. B., Glöckner, C. et al. (2016). Structural characterization suggests models for monomeric and dimeric forms of full-length ezrin. *Biochem. J.* **473**, 2763-2782. doi:10.1042/BCJ20160541

Roland, B. P., Naito, T., Best, J. T., Arnaiz-Yépez, C., Takatsu, H., Yu, R. J., Shin, H.-W. and Graham, T. R. (2019). Yeast and human P4-ATPases transport glycosphingolipids using conserved structural motifs. *J. Biol. Chem.* **294**, 1794-1806. doi:10.1074/jbc.RA118.005876

Sánchez-Madrid, F. and Serrador, J. M. (2009). Bringing up the rear: defining the roles of the uropod. *Nat. Rev. Mol. Cell Biol.* **10**, 353-359. doi:10.1038/nrm2680

Serrador, J. M., Alonso-Lebrero, J. L., del Pozo, M. A., Furthmayr, H., Schwartz-Albiez, R., Calvo, J., Lozano, F. and Sánchez-Madrid, F. (1997). Moesin interacts with the cytoplasmic region of intercellular adhesion molecule-3 and is redistributed to the uropod of T lymphocytes during cell polarization. *J. Cell Biol.* **138**, 1409-1423. doi:10.1083/jcb.138.6.1409

Serrador, J. M., Nieto, M., Alonso-Lebrero, J. L., del Pozo, M. A., Calvo, J., Furthmayr, H., Schwartz-Albiez, R., Lozano, F., González-Amaro, R., Sánchez-Mateos, P. et al. (1998). CD43 interacts with moesin and ezrin and regulates its redistribution to the uropods of T lymphocytes at the cell-cell contacts. *Blood* **91**, 4632-4644. doi:10.1182/blood.V91.12.4632

Serrador, J. M., Urzainqui, A., Alonso-Lebrero, J. L., Cabrero, J. R., Montoya, M. C., Vicente-Manzanares, M., Yáñez-Mó, M. and Sánchez-Madrid, F. (2002). A juxta-membrane amino acid sequence of P-selectin glycoprotein ligand-1 is involved in moesin binding and ezrin/radixin/moesin-directed targeting at the trailing edge of migrating lymphocytes. *Eur. J. Immunol.* **32**, 1560-1566. doi:10.1002/1521-4141(200206)32:6<1560::AID-IMMU1560>3.0.CO;2-U

Shin, H.-W. and Takatsu, H. (2019). Substrates of P4-ATPases: beyond aminophospholipids (phosphatidylserine and phosphatidylethanolamine). *FASEB J.* **33**, 3087-3096. doi:10.1096/fj.201801873R

Shin, H.-W., Morinaga, N., Noda, M. and Nakayama, K. (2004). BIG2, a guanine nucleotide exchange factor for ADP-ribosylation factors: its localization to recycling endosomes and implication in the endosome integrity. *Mol. Biol. Cell* **15**, 5283-5294. doi:10.1091/mbc.e04-05-0388

Simons, P. C., Pietromonaco, S. F., Reczek, D., Bretscher, A. and Elias, L. (1998). C-terminal threonine phosphorylation activates ERM proteins to link the cell's cortical lipid bilayer to the cytoskeleton. *Biochem. Biophys. Res. Commun.* **253**, 561-565. doi:10.1006/bbrc.1998.9823

Takada, N., Takatsu, H., Miyano, R., Nakayama, K. and Shin, H.-W. (2015). ATP11C mutation is responsible for the defect in phosphatidylserine uptake in UPS-1 cells. *J. Lipid Res.* **56**, 2151-2157. doi:10.1194/jlr.M062547

Takai, Y., Kitano, K., Terawaki, S.-I., Maesaki, R. and Hakoshima, T. (2007). Structural basis of PSGL-1 binding to ERM proteins. *Genes Cells* **12**, 1329-1338. doi:10.1111/j.1365-2443.2007.01137.x

Takatsu, H., Baba, K., Shima, T., Umino, H., Kato, U., Umeda, M., Nakayama, K. and Shin, H.-W. (2011). ATP9B, a P4-ATPase (a Putative Aminophospholipid Translocase), Localizes to the trans-Golgi Network in a CDC50 Protein-independent Manner. *J. Biol. Chem.* **286**, 38159-38167. doi:10.1074/jbc.M111.281006

Takatsu, H., Tanaka, G., Segawa, K., Suzuki, J., Nagata, S., Nakayama, K. and Shin, H.-W. (2014). Phospholipid flippase activities and substrate specificities of human type IV P-type ATPases localized to the plasma membrane. *J. Biol. Chem.* **289**, 33543-33556. doi:10.1074/jbc.M114.593012

Takatsu, H., Takayama, M., Naito, T., Takada, N., Tsumagari, K., Ishihama, Y., Nakayama, K. and Shin, H.-W. (2017). Phospholipid flippase ATP11C is endocytosed and downregulated following Ca2+-mediated protein kinase C activation. *Nat. Commun.* **8**, 1423. doi:10.1038/s41467-017-01338-1

Takayama, M., Takatsu, H., Hamamoto, A., Inoue, H., Naito, T., Nakayama, K. and Shin, H.-W. (2019). The cytoplasmic C-terminal region of the ATP11C variant determines its localization at the polarized plasma membrane. *J. Cell Sci.* **132**, jcs231720. doi:10.1242/jcs.231720

Takeuchi, K., Sato, N., Kasahara, H., Funayama, N., Nagafuchi, A., Yonemura, S., Tsukita, S. and Tsukita, S. (1994). Perturbation of cell adhesion and microvilli formation by antisense oligonucleotides to ERM family members. *J. Cell Biol.* **125**, 1371-1384. doi:10.1083/jcb.125.6.1371

Tanaka, Y., Ono, N., Shima, T., Tanaka, G., Katoh, Y., Nakayama, K., Takatsu, H. and Shin, H.-W. (2016). The phospholipid flippase ATP9A is required for the recycling pathway from the endosomes to the plasma membrane. *Mol. Biol. Cell* **27**, 3883-3893. doi:10.1091/mbc.E16-08-0586

Terawaki, S., Maesaki, R. and Hakoshima, T. (2006). Structural basis for NHERF recognition by ERM proteins. *Structure* **14**, 777-789. doi:10.1016/j.str.2006.01.015

Thomas, S., Ritter, B., Verbich, D., Sanson, C., Bourbonnière, L., McKinney, R. A. and McPherson, P. S. (2009). Intersectin regulates dendritic spine development and somatodendritic endocytosis but not synaptic vesicle recycling in hippocampal neurons. *J. Biol. Chem.* **284**, 12410-12419. doi:10.1074/jbc.M809746200

Tsukita, S. and Yonemura, S. (1999). Cortical actin organization: lessons from ERM (ezrin/radixin/moesin) proteins. *J. Biol. Chem.* **274**, 34507-34510. doi:10.1074/jbc.274.49.34507

Tsukita, S., Oishi, K., Sato, N., Sagara, J., Kawai, A. and Tsukita, S. (1994). ERM family members as molecular linkers between the cell surface glycoprotein CD44 and actin-based cytoskeletons. *J. Cell Biol.* **126**, 391-401. doi:10.1083/jcb.126.2.391

Turunen, O., Wahlström, T. and Vaheri, A. (1994). Ezrin has a COOH-terminal actin-binding site that is conserved in the ezrin protein family. *J. Cell Biol.* **126**, 1445-1453. doi:10.1083/jcb.126.6.1445

Valderrama, F., Thevapala, S. and Ridley, A. J. (2012). Radixin regulates cell migration and cell-cell adhesion through Rac1. *J. Cell Sci.* **125**, 3310-3319. doi:10.1242/jcs.094383

Valignat, M.-P., Nègre, P., Cadra, S., Lellouch, A. C., Gallet, F., Hénon, S. and Theodoly, O. (2014). Lymphocytes can self-steer passively with wind vane uropods. *Nat. Commun.* **5**, 5213. doi:10.1038/ncomms6213

Wehman, A. M., Poggioli, C., Schweinsberg, P., Grant, B. D. and Nance, J. (2011). The P4-ATPase TAT-5 inhibits the budding of extracellular vesicles in C. elegans embryos. *Curr. Biol.* **21**, 1951-1959. doi:10.1016/j.cub.2011.10.040

Wei, C., Wang, X., Zheng, M. and Cheng, H. (2012). Calcium gradients underlying cell migration. *Curr. Opin. Cell Biol.* **24**, 254-261. doi:10.1016/j.ceb.2011.12.002

Welf, E. S., Miles, C. E., Huh, J., Sapoznik, E., Chi, J., Driscoll, M. K., Isogai, T., Noh, J., Weems, A. D., Pohlkamp, T. et al. (2020). Actin-membrane release initiates cell protrusions. *Dev. Cell* **55**, 723-736.e8. doi:10.1016/j.devcel.2020.11.024

Yang, H. W., Collins, S. R. and Meyer, T. (2016). Locally excitable Cdc42 signals steer cells during chemotaxis. *Nat. Cell Biol.* **18**, 191-201. doi:10.1038/ncb3292

Yonemura, S., Hirao, M., Doi, Y., Takahashi, N., Kondo, T., Tsukita, S. and Tsukita, S. (1998). Ezrin/radixin/moesin (ERM) proteins bind to a positively charged amino acid cluster in the juxta-membrane cytoplasmic domain of CD44, CD43, and ICAM-2. *J. Cell Biol.* **140**, 885-895. doi:10.1083/jcb.140.4.885

Zhang, Y., Werling, U. and Edelmann, W. (2012). SLiCE: a novel bacterial cell extract-based DNA cloning method. *Nucleic Acids Res.* **40**, e55. doi:10.1093/nar/gkr1288

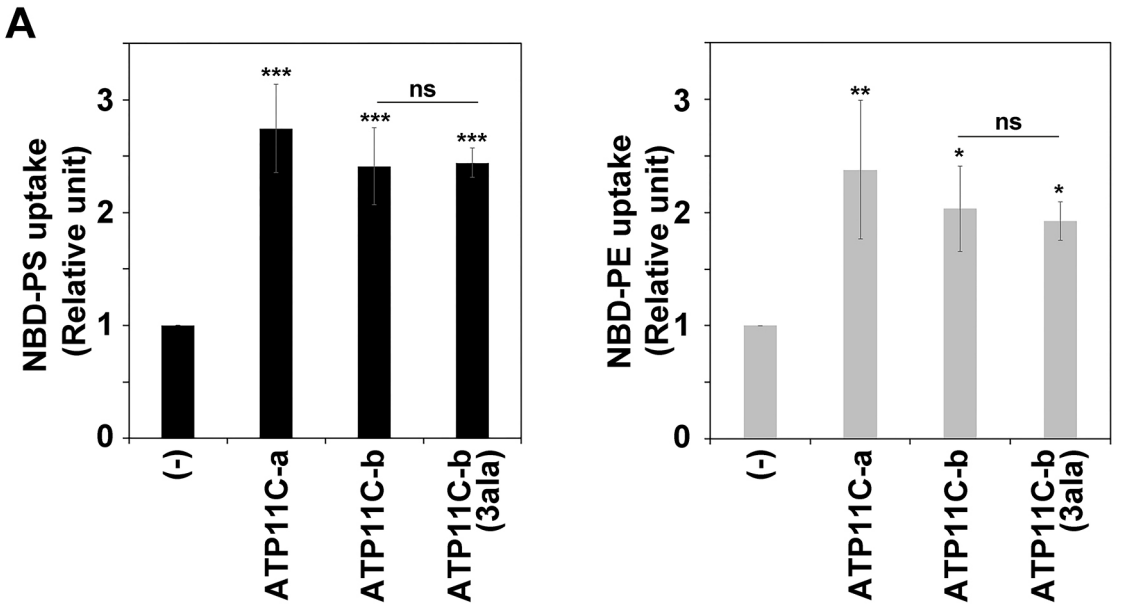

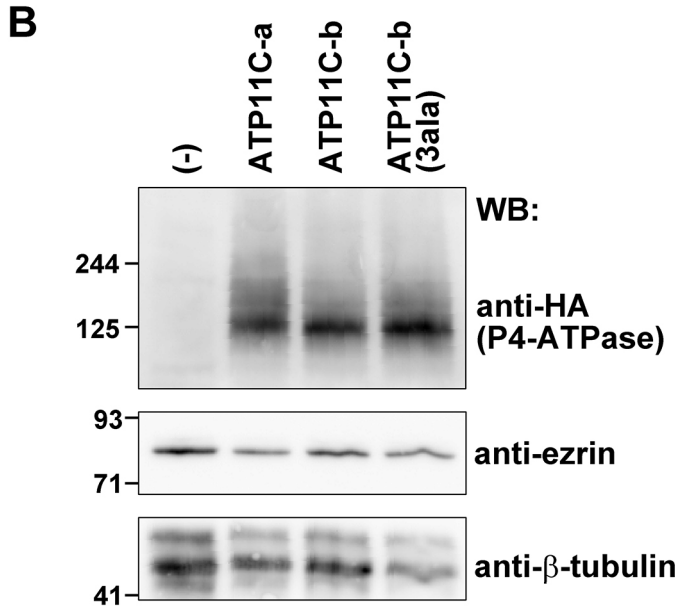

Supplementary Figure S1 Inoue & Takatsu

Fig. S1. Comparison of flippase activity between ATP11C-a, ATP11C-b, and ATP11C-b(3ala)-expressing cells. (A) Parental MDA-MB-231 cells (-) and MDA-MB- 231 cells stably expressing ATP11C-a, ATP11C-b, or ATP11C-b(3ala) were washed with flippase assay buffer and incubated with NBD-labelled lipids (NBD-PS for 5 min or NBE-PE for 15 min) at 15°C. After extraction with fatty acid-free BSA, the residual fluorescence intensity of the cells was measured by flow cytometry. Uptake of NBD-labelled lipids is shown relative to parental cells (-). Graphs ± SD display the average of three independent experiments. Variance was assessed by comparison of all pairs using a Student's *t*-test. * $p < 0.05$, ** $p < 0.01$, *** $p < 0.001$, ns not significant. **(B)** MDA-MB- 231 cells stably expressing ATP11C-a, ATP11C-b, or ATP11C-b(3ala), and parental cells (-), were lysed and subjected to immunoblotting using anti-H A, anti-ezrin, or anti-β-actin antibodies.

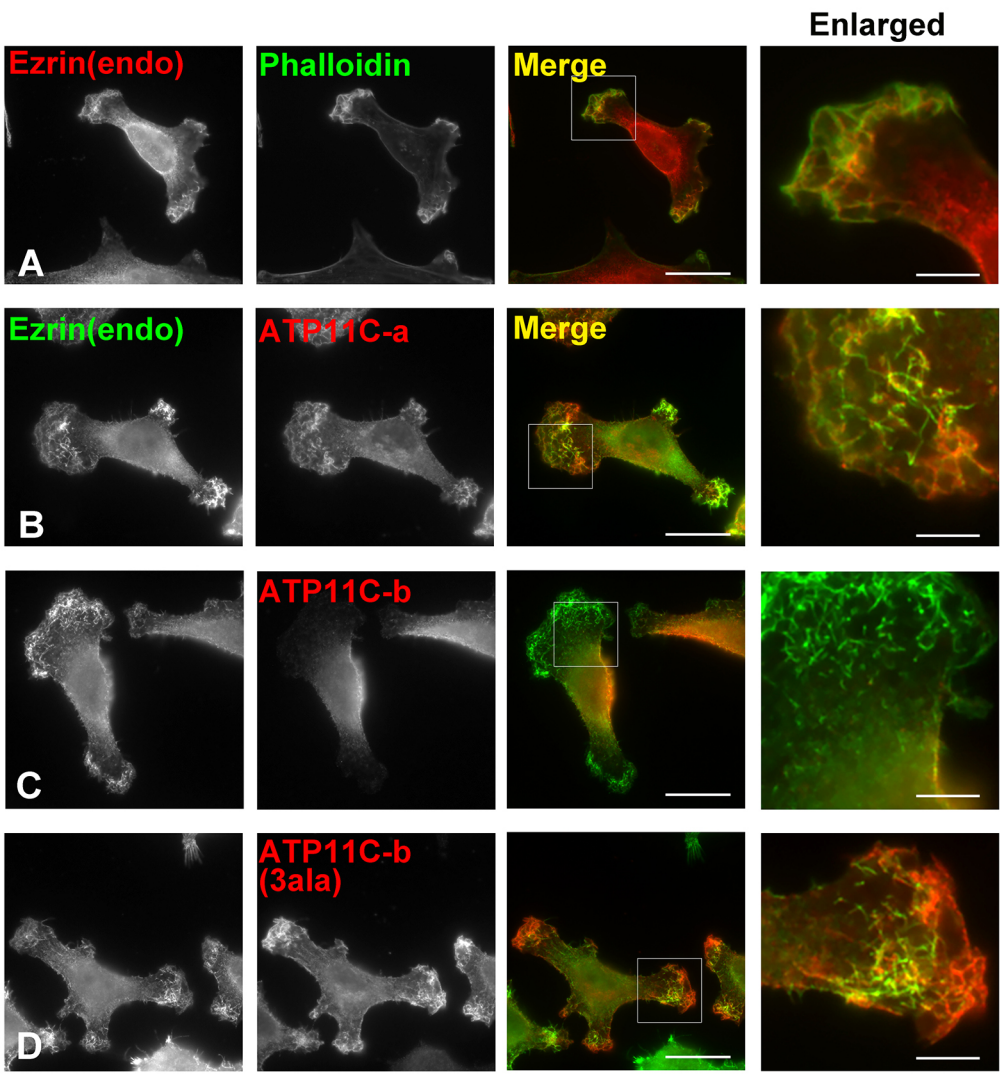

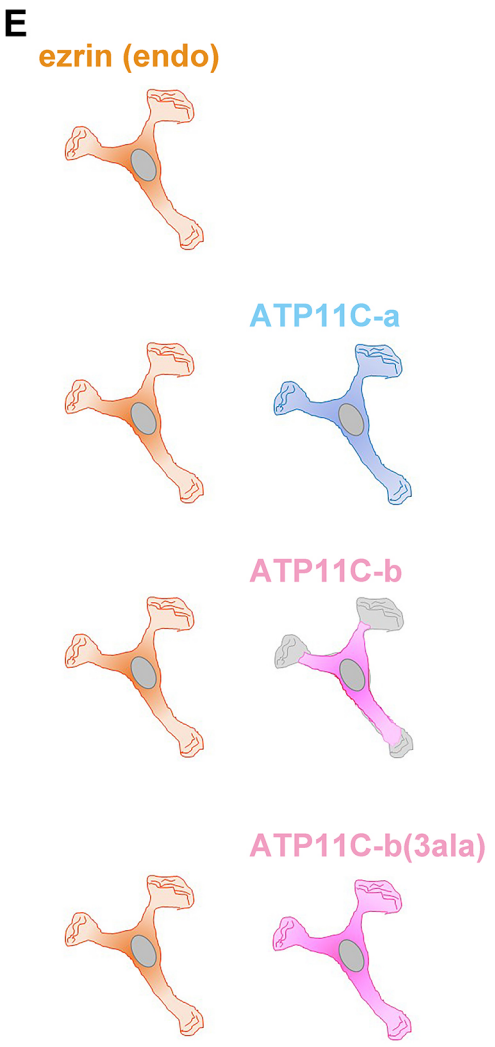

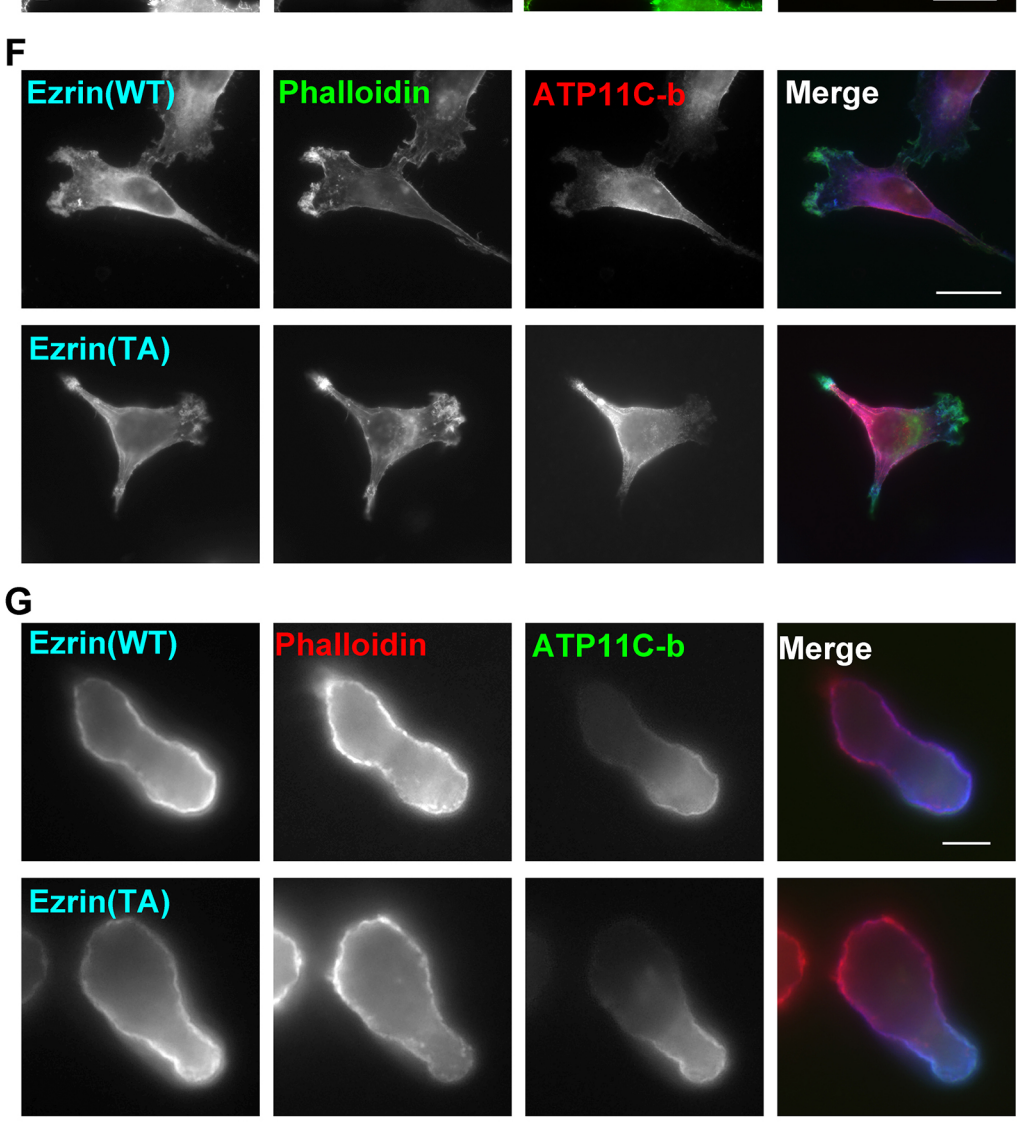

Supplementary Figure S2 Inoue & Takatsu

Fig. S2. Localization of endogenous ezrin in cells expressing ATP11C-a, ATP11C-b, or ATP11C-b(3ala). (A) Parental MDA-MB-231 cells (-) and MDA-MB-231 cells stably expressing **(B)** ATP11C-a, **(C)** ATP11C-b, or **(D)** ATP11C-b(3ala) were fixed and immunostained using anti-ezrin alone **(A)** or anti-ezrin and anti-HA antibodies **(B-D)** followed by incubation with Alexa555-conjugated anti-mouse secondary antibody and Alexa488-conjugated phalloidin **(A)** or Alexa488-conjugated anti-mouse and Cy3-conjugated anti-rat secondary antibodies **(B-D)**. Scale bars, 20 μm. Scale bars in enlarged images, 5 μm. **(E)** Schematic illustration of localization of endogenous ezrin and each ATP11C isoform and corresponding mutants. Orange, endogenous ezrin; light blue, ATP11C-a; pink, ATP11C-b. **(F)** MDA-MB-231 cells and **(G)** BaF3 cells stably co-expressing HA-tagged ATP11C-b and FLAG-tagged ezrin(WT) or ezrin(T567A) (TA) were fixed and stained for HA and FLAG followed by incubation with Cy3-conjugated anti-rat and DyLight649-conjugated anti-mouse secondary antibodies and Alexa488-conjugated phalloidin **(F)**, or Alexa488-conjugated anti-rat and DyLight649-conjugated anti-mouse secondary antibody and Alexa555-conjugated phalloidin **(G)**. Scale bars, 20 μm **(F)** and 5 μm **(G).**

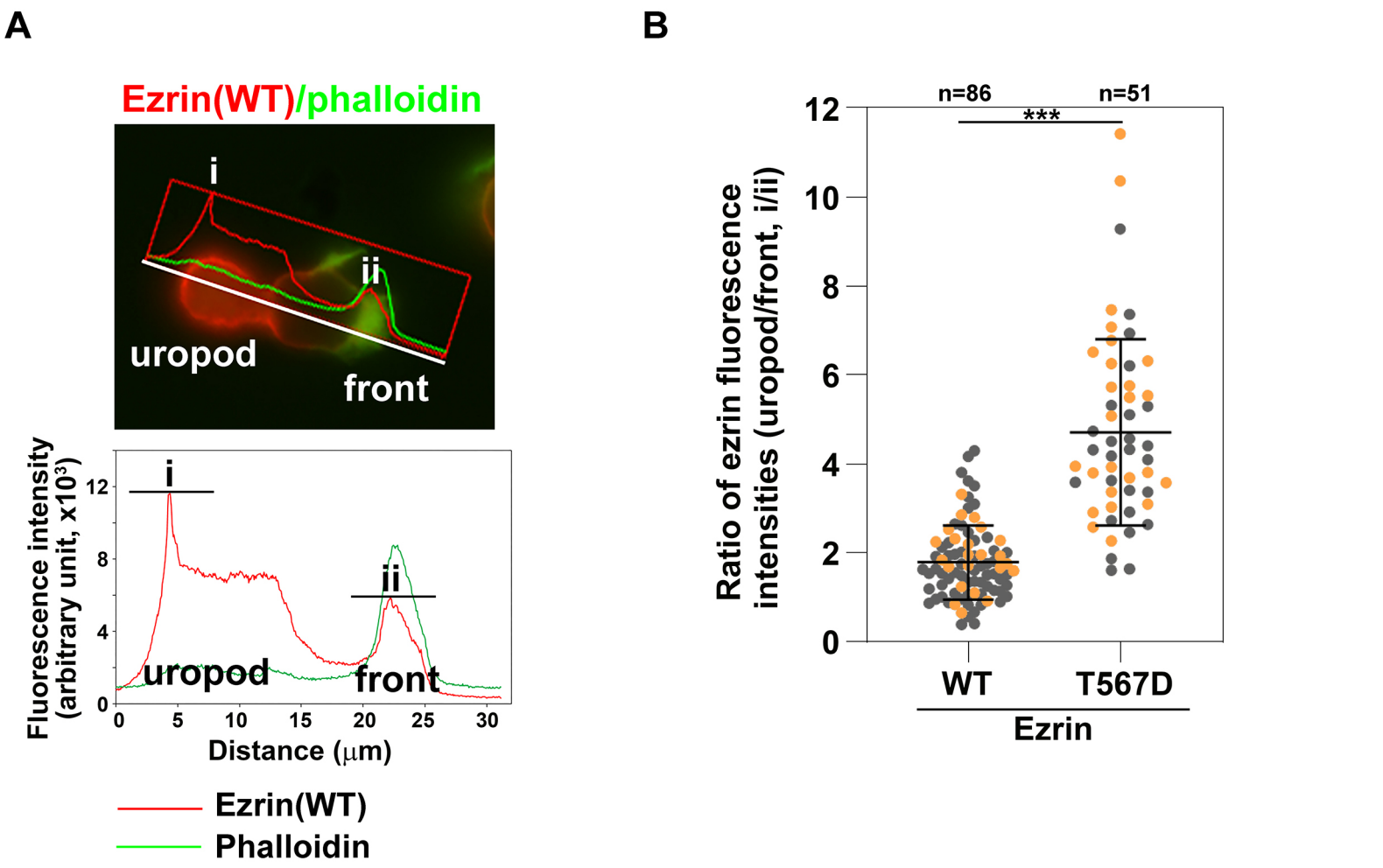

Supplementary Figure S3 Inoue & Takatsu

Fig. S3. Estimation of polarized localization of ezrin(WT) and the phosphomimetic ezrin mutant. (A) A representative line-scan profile from the uropod to the front of a BaF3 cell expressing ezrin(WT). The line scan was performed using the ZEN software. **(B)** The ratio of the peak fluorescence intensity of the uropod to front (i/ii) of a BaF3 cell expressing ezrin(WT) or ezrin(T567D) was calculated and expressed as scatter plots, as described in the legend for Figure 6D. Individual dots represent the ratios in individual cells. Graphs ± SD display the average ratio from all analyzed cells, and 'n' is the total number of analyzed cells from two independent experiments. Variance was assessed by comparison between ezrin(WT) and ezrin(T567D) using a Student's *t*-test. *** $p < 0.0001$.

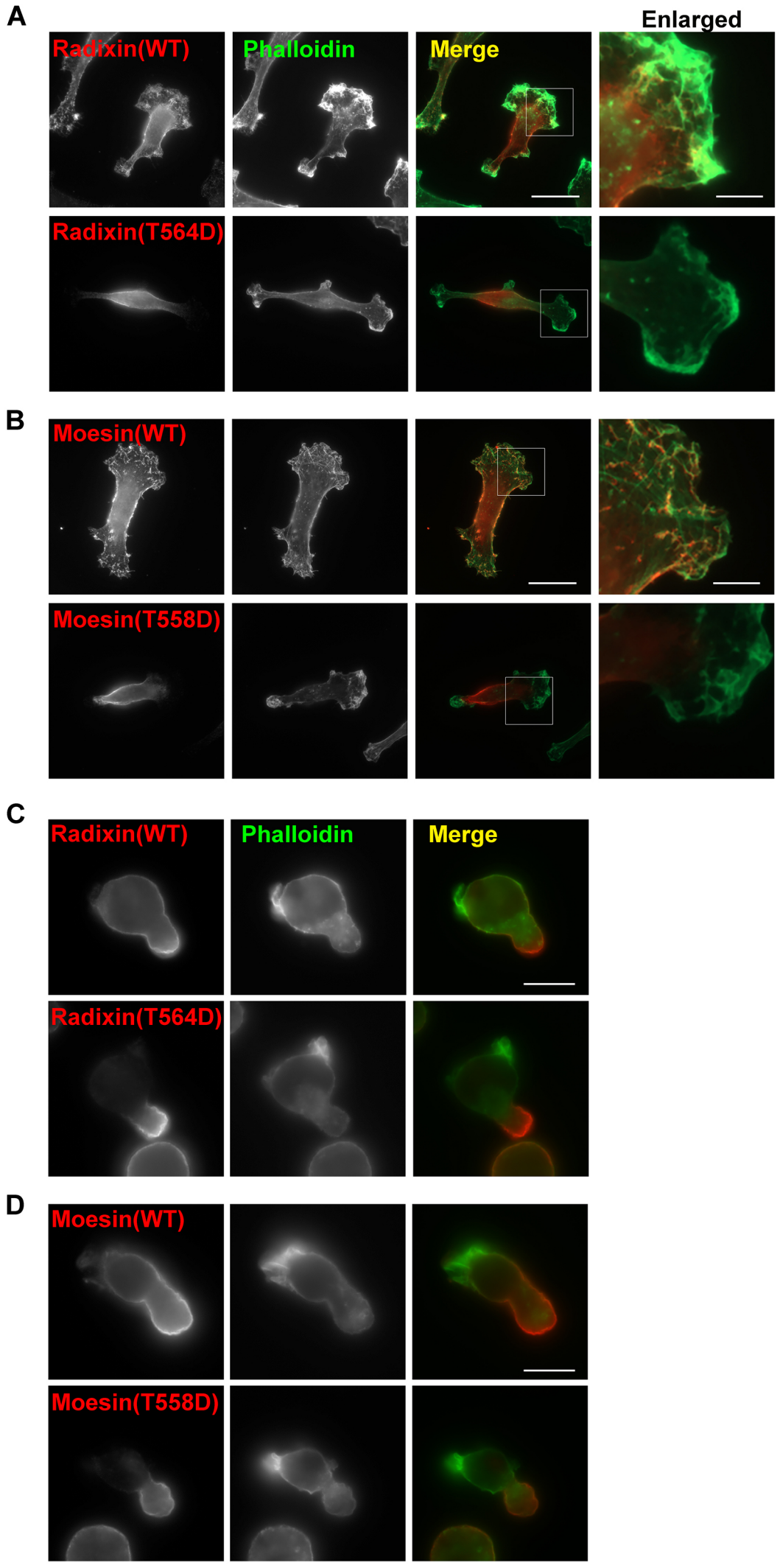

Supplementary Figure S4 Inoue & Takatsu

Fig. S4. Polarized localization of the phosphomimetic radixin and moesin mutants. (A, B) MDA-MB-231 cells and **(C, D)** BaF3 cells stably expressing C-terminally FLAG-tagged radixin(WT), radixin(T564D), moesin(WT), or moesin(T558D) were fixed and stained for FLAG followed by incubation with Alexa555-conjugated anti-mouse secondary antibody and Alexa488-conjugated phalloidin. Scale bars, 20 μm, 5 μm in enlarged images **(A, B)**, and 10 μm **(C, D)**.

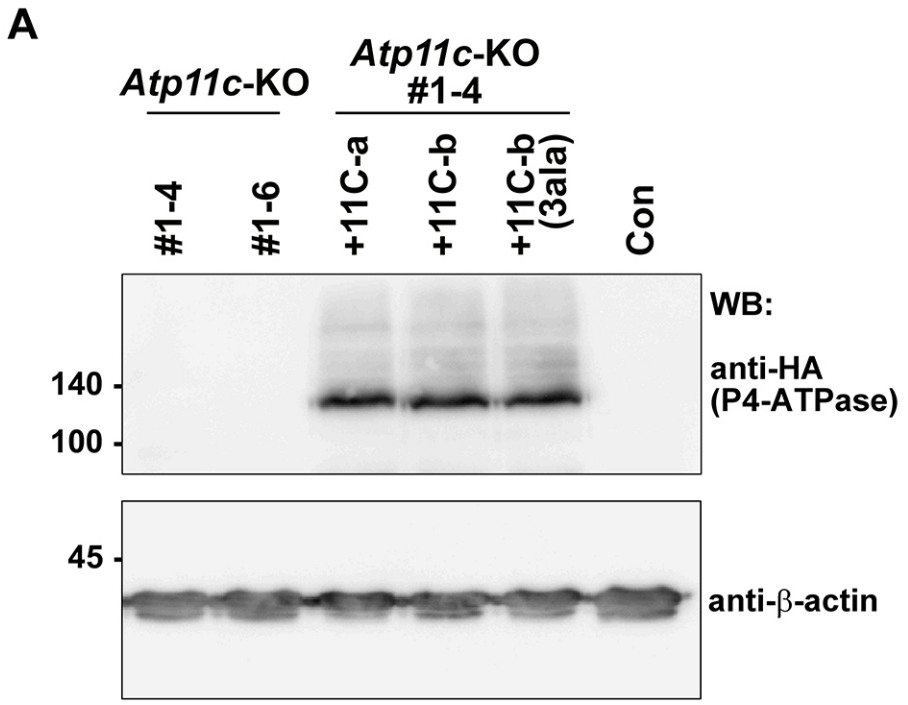

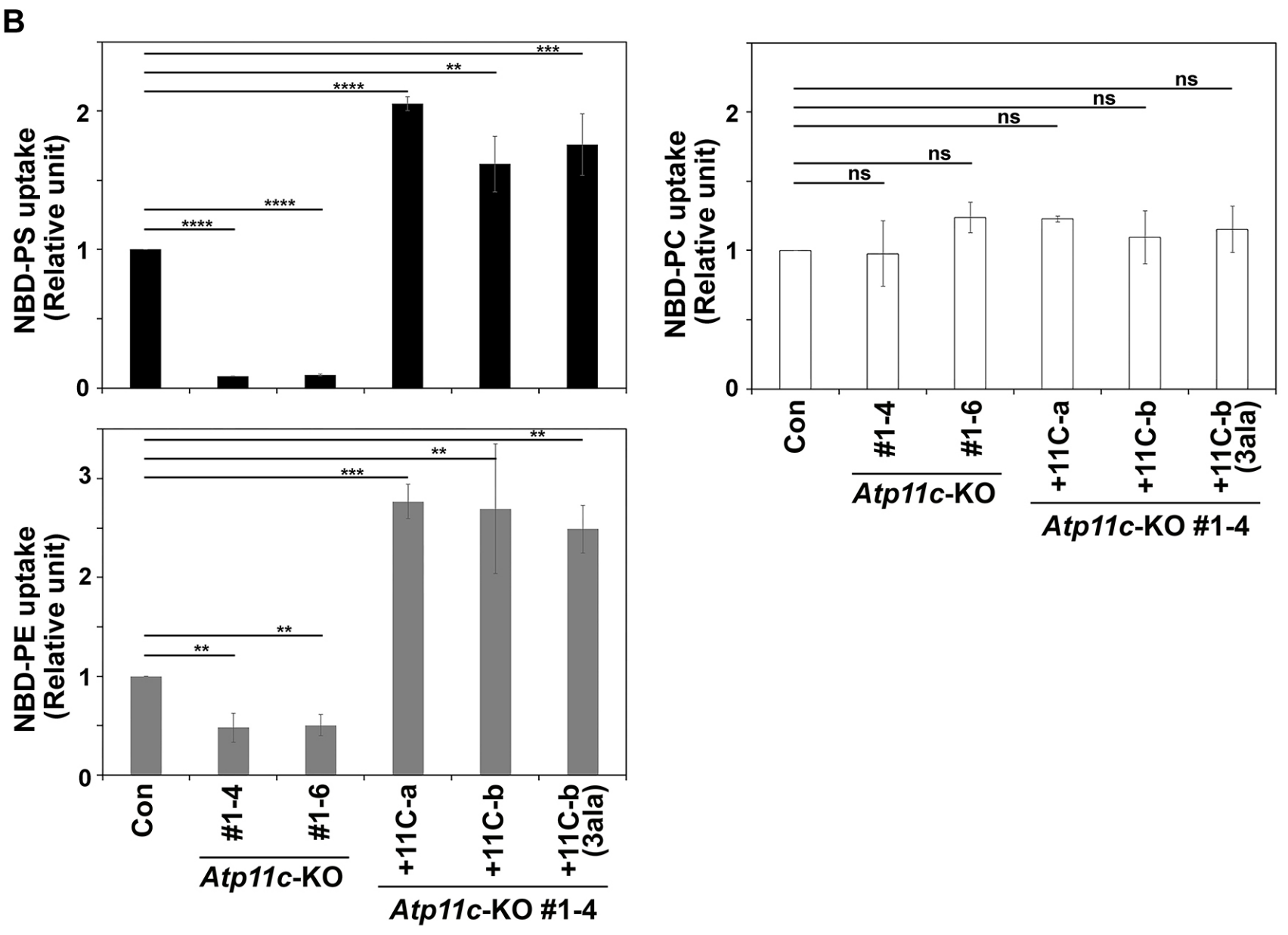

Supplementary Figure S5 Inoue & Takatsu

Fig. S5. Expression of exogenous ATP11C-a, ATP11C-b, and ATP11C-b(3ala) in *Atp11c*-knockout cells. (A) Parental BaF3 cells (Con), *Atp11c*-knockout cells, and cells stably expressing CRISPR-resistant HA-tagged ATP11C-a, ATP11C-b, or ATP11C-b(3ala) in the indicated *Atp11c*-knockout cell clone were lysed, and lysates were subjected to SDS-PAGE and immunoblotting using anti-HA or anti-β-actin (as an internal control) antibodies. **(B)** Cells in **(A)** were washed with flippase assay buffer and incubated with NBD-PS for 5 min, NBD-PE for 15 min, or NBD-PC for 15 min at 15°C. After extraction with fatty acid-free BSA, cellular fluorescence intensity was measured by flow cytometry. Uptake of NBD-conjugated lipids is shown relative to parental cells (Con). Graphs ± SD display the average of three independent experiments. A one-way ANOVA was performed to assess variance, and comparisons to parental cells (Con) were made with Dunnett's analysis. ** $p < 0.01$, *** $p < 0.001$, **** $p < 0.0001$.

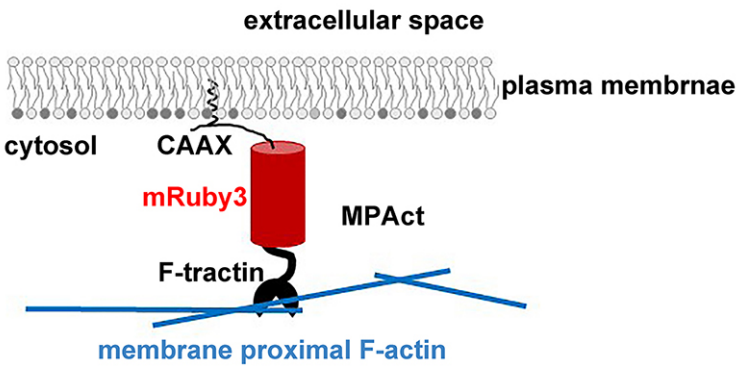

Fig. S6. MPAct probe recognizes membrane proximal F-actin (Bisaria et al., 2020)

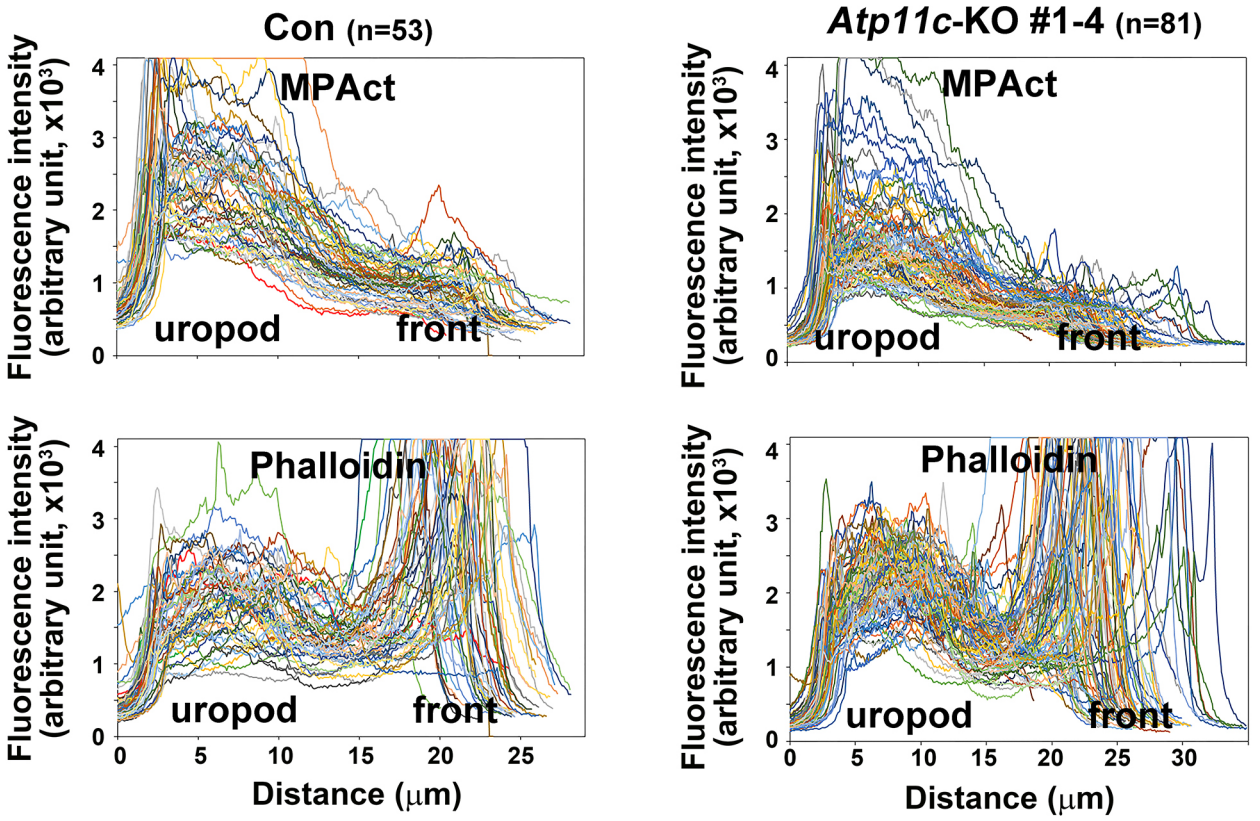

Supplementary Figure S7 Inoue & Takatsu

Fig. S7. Enrichment of MPAct at the uropod in BaF3 cells

Parental BaF3 cells (Con) and *Atp11c*-knockout cells stably expressing MPAct-mRuby3 were fixed and incubated with Alexa488-conjugated phalloidin. Line-scan profiles of MPAct and phalloidin fluorescence from the uropod to the front of these cells are shown. Different colors of lines represent different cells and 'n' is the total number of analyzed cells.